Spectrum Sharing with Device-to-Device Successive Relaying and Hybrid Complex Field Network Coding

Chao Ren, *Student Member, IEEE,* Jian Chen, *Member, IEEE* and Chintha Tellambura, *Fellow, IEEE,*

***Abstract*—While device-to-device (D2D) communication between two proximate cellular terminals improves spectral efficiency, cooperative spectrum sharing (CSS) among D2D users (DUs) and cellular users (CUs) provides more gains. In this paper, we thus propose a new CSS scheme, where a pair of DUs (D_1 and D_2) acts as half-duplex two-path successive relays (TPSRs) between two CUs (C_1 and C_2) while maintaining cellular full-duplex gains. The channel between D_1 and D_2, referred to as TPSR inter-relay interference channel, is exploited to provide D2D access with an ideal throughput of 1 symbol per time slot (sym/TS). To eliminate the interference between C_1-C_2 and D_1-D_2 links, we propose a hybrid complex field network coding (HCFNC) scheme for two cases: 1) both of D_1 and D_2 correctly decode cellular data, and 2) either D_1 or D_2 correctly decodes cellular data. For each case, we derive the closed-form CU diversity-multiplexing tradeoff (DMT) and data rate, symbol error probability (SEP) for the HCFNC strategy, and the D2D throughput. Our performance analysis and simulation results show that: 1) the proposed scheme achieves the 3×1 multiple-input single-output (MISO) DMT; 2) the CU achievable rate approaches the full-duplex upper bound; 3) the DU average throughput approaches 1 sym/TS at high signal-to-interference-plus-noise ratio (SINR), demonstrating that DUs gain full access opportunity to the cellular spectrum.**

***Index Terms*—Device-to-device, cooperative spectrum sharing, complex field network coding, successive relaying, diversity-multiplexing tradeoff.**

I. Introduction

Device-to-Device (D2D) communication, an underlay paradigm [1], fulfills the urgent demand of proximity service (ProSe) among highly-capable user equipments (UEs) [2]. It has been proposed for the third generation partnership project (3GPP) long-term evolution (LTE) standard and can facilitate peer-to-peer applications, social networking, e-commerce, machine type communication, advertising and other applications [3]. It provides *hop gain*, *proximity gain* and *reuse gain* [4]. The first two gains quantify the ability to achieve high-rates and low-power data exchange for near D2D users (DUs). The reuse gain quantifies the simultaneous spectrum usage by both cellular users (CUs) and DUs. These three gains show that the DU pairs achieve efficient intra-cell access for themselves by sharing the cellular spectrum.

Although simultaneous sharing of frequency resources clearly improves the total spectral efficiency [5], [6], the problem is intra-cell interference (ICI) between cellular and D2D links [2], [4], [7]. In this context, D2D is similar to spectrum sharing cognitive radio (CR) [8], [9]. Nevertheless, for both these systems, not only ICI, but also the lack of incentive or even "inherently hostility" [10] of priority users (i.e., the primary users (PUs) and CUs) to share their spectrum is one of the major problems [9]–[11]. Thus, incentivizing them to share spectrum with secondary users (SUs) or DUs is a key challenge [9], [11].

To answer this challenge and to mitigate the ICI, cooperative spectrum sharing (CSS) is developed for D2D [2], [7]–[9], [12], [13]. The potential benefits of are diversity gains, coverage extension and energy savings [14]–[17]. Thus, in return for relaying CU messages, DUs can access the cellular spectrum [8]. Furthermore, utilizing wireless broadcasting, the ICI channel becomes the basis of establishing in-band cooperation, and the adverse effects of ICI can also be partially mitigated. Moreover, CSS D2D is relatively simple to implement when both the DUs and CUs belong to the same cellular network. For example, the existing infrastructure helps to acquire channel state information (CSI), to set up links and so on.

Nevertheless, the existing D2D CSS schemes [2], [7], [8], [12], [13] are adversely affected by (A) low CU diversity gain, (B) half-duplex loss due to conventional relaying and (C) self-interference and inter-relay interference (IRI). The reasons for (A) are non-utilization of CU-to-CU direct path and interference between DU and CU links. The reason for (B) is that half-duplex relaying uses two time slots per data exchange. The reason for (C) is that the use of full-duplex relaying, superposition-coding and successive relaying generates relatively large interference compared to the power of desired signal, which severely degrades the spectral efficiency and diversity gain. In addition, the low ratio (we refer to this metric in CSS as participation ratio) of participant DUs used as CU relays results in (a) relatively low cellular diversity order and (b) few cellular and D2D communication phases. To counteract (a), we exploit spatial diversity by utilizing more DUs to create more independent relaying paths. For (b), if more DUs participate in CSS, increased communication phases provide flexibility to transmit CU data and DU data. Thus, careful protocol design potentially yields benefits for both CUs and DUs.

This work was supported by National Natural Science Foundation of China under Grant 61601347, in part by the 111 project of China under Grant B38038 and in part by the scholarship from China Scholarship Council under grant 201506960024. (Corresponding author: Chintha Tellambura).

C. Ren and J. Chen are with the State Key Laboratory of Integrated Services Networks, Xidian University, Xian 710071, China (e-mail: renchao@stu.xidian.edu.cn; jianchen@mail.xidian.edu.cn).

C. Tellambura is with the Department of Electrical and Computer Engineering, University of Alberta, Edmonton, AB, Canada T6G 2V4. (chintha@ece.ualberta.ca).

TABLE I
COMPARISON OF RELATED CSS WORKS.

Related Works	Relaying Type	Direct-Path	CU Diversity (d) and Multiplexing (r) Gains	Number and Ratio of Participated DUs	Interference Mitigation	CU Priority
[2]	HDR	Yes	$^*d = 2$ and $r = \frac{1}{2}$	1 in 2, 50%	Stored cancellation	No
[7]	FDR	Yes	$^*d = 2$ and $r = 1$	1 in 2, 50%	No	Min-rate
[8]	TWR	No	$^*d = 1$ and $r = 1$	2 in 2, 100%	No	No
[12]	TPSR	Yes	$^*d = 2$ and $r = 1$	2 in 4, 50%	No	No
[13]	TWR	No	$^*d = 1$ and $r = 1$	1 in 2, 50%	CIOD	Interference-free
Proposed	TPSR	Yes	$d = 3$ and $r = 1$	2 in 2, 100%	HCFNC	Interference-free

A. Contributions

To alleviate the aforementioned problems, we propose a successive spectrum sharing (SSS) scheme (Fig. 1), where two DUs, say, D_1 and D_2 act as relays for a pair of CUs while simultaneously accessing the cellular spectrum. The main features and details are as follows:

1) **Cellular diversity-multiplexing tradeoff (DMT)**. Because the DUs cooperate and also utilize the cellular direct-path, the CU link achieves the 3×1 multiple-input single-output (MISO) DMT.
2) **Cellular interference elimination**. To create an interference-free CU channel, we propose a hybrid complex field network coding (HCFNC) technique, thereby fully eliminating the error-floor.
3) **Virtual full-duplex relaying**. The pair of DUs forms a 'virtual full-duplex' two-path successive relaying (TPSR) mode, where D_1 and D_2 alternate between transmission and reception phases. CU's half-duplex loss is compensated because only one time slot is needed per data transmission.
4) **Cellular Priority**. Interference-elimination, full diversity and full-duplex multiplexing are prioritized and guaranteed for the CUs.
5) **D2D full spectrum access opportunity and full participation**. Since D_1 and D_2 communicate alternatively in successive slots, IRI between them also exists. But we exploit the IRI channel to provide data exchange for DUs in each time slot. Thus, the proposed SSS scheme utilizes all time resources for DUs on this band, and provides full spectrum access opportunity for DUs. On the other hand, all DU participation as CU relays benefits both CU communication and the D2D full spectrum access.

This paper discusses two cases: Case I - both the DUs can decode; Case II - only one DU can decode. For each case, we analyze the CU achievable DMT and data rate, DU symbol error probability (SEP) with HCFNC, and the D2D throughput. Specifically, because signal constellation based approaches are sensitive to the channel-phase estimation error (PEE) [18], it is fully considered in our derivations of the CU achievable rate in Case I.

B. Related Works

The first CSS model studied the achievable rate region of PU and SU in an information-theoretic perspective for CR networks [19], [20]. Reference [21] introduced D2D relaying concept to improve cellular multicast services. Primarily in a D2D scenario, Li *et al*. [22] raised the cooperation concept that utilizes the base station (BS) as an incremental D2D relay to enhance the D2D performance. However, no gains are available to the CUs, and moreover the D2D hop gain degrades since both uplink and downlink are needed [7]. Therefore, to mutually benefit both DUs and CUs by improving spectral efficiency, CSS makes sense for D2D scenarios.

We compare and summarize related CSS works [2], [7], [8], [12], [13] and this work in Table I (in this table, * means these gains have not been proved by the authors, but we have estimated them by assuming perfect interference mitigation; 'Participated DUs' stands for x out of y DUs can be employed to relay CU data).

Specifically, in [2], [7], [8], [12], one DU from the D2D pair codes its own signal on to the cellular signal via a superposition code in a time slot and relays the coded signal to both DU and CU in the next time slot. The interference signal from CU can be decoded and kept by DU, which can be utilized for 'stored cancellation' in the next time slot. In [2], the DU can access spectrum as long as relaying cellular data in even time slots, but the cellular capacity is limited by half-duplex relaying (HDR). Note that the cellular direct-path is allowed, and the potential diversity order becomes two for the cellular link. In [8], DU serves as an analog network coding (ANC) two-way relay (TWR) [23] for cellular transmissions, improving the cellular capacity which is limited by the half-duplex constraint. In return, D2D data exchange is allowed by the cellular network in each time slot. However, the ANC TWR cannot exploit the direct-path (if exists) [24], [25], and the potential CU diversity order is thus limited to one. To further improve the spectral efficiency, [7] generalized [2] to full-duplex CSS. In this model, the selected DU is a full-duplex relay (FDR) and thus can access the spectrum and relay simultaneously. Although full-duplex DU relaying helps CU transmission, improves cellular capacity and potentially achieves a CU diversity of two, the full-duplex transmissions create self-interference that cannot be completely eliminated, which degrades the system performance [26], [27]. Except for full-duplex relaying, an interesting 'virtual full-duplex' approach called TPSR [28], [29] has been evolved to cognitive CSS by [12], and note that the cognitive CSS is similar to D2D CSS. To incorporate TPSR concept in this model, two of four SUs are utilized as half-duplex relays to alternatively help forward the PU signal. Simultaneously, the PU can continue transmissions without waiting for the finish of two-hop relaying process. Special self-interference links in TPSR, namely IRI links, are utilized to provide data exchange for SUs, which is a remarkable difference between 'virtual full-duplex' CSS

and full-duplex CSS [7] on how to treat interference. With the cellular direct-path, the potential diversity for this scheme can be two if inter-user interference is canceled perfectly.

The main differences between works [2], [7], [8], [12] and this work can be found in Table I. Although these CSS schemes are win-win strategies, a critical problem is that every node must detect its desired signal in the presence of interference of the superposition-coded signals intended for other users [13]. This interference results in an irreducible error-floor and signal-to-interference-plus-noise ratio (SINR) floor, dramatically increasing the error probability [13] and consequently limiting diversity gain and capacity. To address this problem, [13] proposed a security-embedded interference avoidance scheme based on constellation rotation [30] and the CSS model [8]. In this scheme [13], the *intrinsic orthogonality* between the real and imaginary components of the complex signal is exploited to realize interference-free CU and DU transmissions. However, the CU diversity order of this schemes is one because the direct-path is not used, and the participation ratio is only 50% since only one DU serves as relay. Thus, this scheme does not provide a 3×1 MISO DMT for the CU link. Despite the higher DU participation ratio and CU DMT, our work is different from [13] in the following key aspects: 1) two DUs in our paper works alternatively as a 'virtual full-duplex relay' for CU, while [13] only employed one DU to realize two-way relaying; 2) in our system model, we consider all possible links, but [13] assumed the DU direct-path and another DU-CU path are absent; 3) more co-channel interferences are generated by those links, and we thus propose HCFNC to detect desired data instead of the original signal space orthogonality or coordinate-interleaved orthogonal design (CIOD) in [13]; 4) PEE is considered in our paper as deriving the achievable rate, which leads to a more practical performance evaluation.

While spectrum leasing for CR [31], [32] is closely related to CSS for D2D, there are prominent differences between these two spectrum sharing models: 1) spectrum leasing shares the access permission of PU and SU in time division multiple access manner, but CSS D2D makes the coexistence of CU and DU on the same time-frequency block possible; and 2) spectrum leasing requires orthogonality in time domain, while conventional CSS D2D uses signal processing techniques for co-channel interference mitigation. Thus, compared with spectrum leasing model [31], the CSS D2D model in our paper can free up time resources at the expense of signal processing (e.g., precoding and detection)[1].

The rest of this paper is organized as follows. The system model is introduced in Section II. In Section III, we describe the SSS scheme (Case I) in detail and propose the HCFNC technique. Performance analyses and numerical results for Case I are presented in Section IV. In Section V, we discuss bidirectional D2D spectrum sharing (Case II) in detail and provide both performance analyses and numerical results. Finally, Section VI draws the conclusion.

Notations: $\Re\{x\}$ and $\Im\{x\}$ denote real and imaginary parts of x. $\mathbb{E}\{x\}$ is statistical expectation of x. Vector $\boldsymbol{x}$ has the i-th element $x(i)$. Matrix $\mathbf{X}$ has the (i,j)-th element $X(i,j)$, and $\mathbf{I}_n$ is the identity matrix of size $n \geq 1$. $\mathbb{R}$ and $\mathbb{C}$ denote real and complex numbers, and $\mathbb{R}^+ = \{x | x > 0, x \in \mathbb{R}\}$.

[1]Complexity analysis is beyond the scope of this paper.

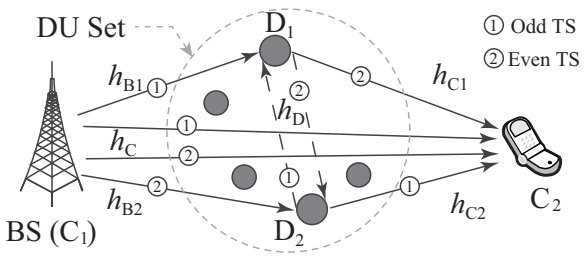

Fig. 1. The system model for SSS scheme.

II. System Model

As per Fig. 1, we consider a typically single cell scenario as [2], [8], [9], [22], where at most one scheduled active D2D pair (D_1 and D_2) attempts to access the same spectrum slot as the cellular pair (BS and C_2).

We assume that the channels remain static during each frame ($L+1$ time slots) [30], [33] and the complex channel coefficients of BS-CU, BS-D_1, BS-D_2, D_1-D_2, D_1-CU, D_2-CU links are denoted by h_C, h_{B1}, h_{B2}, h_D, h_{C1}, h_{C2}, respectively. As in [13], [33], we assume the channel gains are reciprocal, i.e., $h_{ij} = h_{ji}$ for node i and node j. This assumption is valid for time-division duplexing systems and low Doppler spread channels, e.g., channel models in the 802.11a/g/n standards [34], [35]. The phase of h_k ($k \in \{C, B1, B2, D, C1, C2\}$) is denoted by $\angle h_k$. The background noise at each node is assumed to be independent additive white Gaussian noise (AWGN) with variance σ^2. The transmit powers of BS and DUs are denoted by P_B and P_D respectively. D_α and D_β are used to indicate the D2D transmitter and receiver at the n-th time slot, where the corresponding DU indexes in Fig. 1 are given as $\alpha = \text{mod}(n,2)+1$ and $\beta = 3-\alpha$. s_B^n, s_α^n and s_β^n are used to denote the original data symbols for BS, D_α and D_β at time slot n, respectively. Moreover, the two communicating DUs are called an *exchanging D2D pair*. We consider omni-directional half-duplex radio nodes only and assume cell-level synchronization among the nodes [12].

In the first time slot, the BS broadcasts to the DUs and CU. In the subsequent time slots, three cases will occur according to whether the DUs can correctly decode CU data or not. The decoding errors may be caused by small-scale fading, shadowing, path loss and diverse detection abilities of different D2D devices.

- Case I: (*Successive spectrum sharing*) In this case, both nodes of the exchanging D2D pair are able to decode (for a large dense network of relays, we can find two nodes satisfying this condition [36]). As per Fig. 1, the exchanging D2D pair of nodes alternate as relays for cellular system. The explicit protocol is described in Section III-A.
  In this case, all BS data is relayed successively by the exchanging D2D pair, which in return also has access opportunity to mutually communicate during consecutive time slots.
- Case II: (*Bidirectional D2D spectrum sharing*) In this case, only one DU from the exchanging D2D pair is able to decode, which we assume is D_1 without loss of generality. As per Fig. 1, the signal flow is identical with Case I. For instance, $|h_{B2}|$ is too small to ensure BS data be decoded correctly, so that the signal propagates over

this channel can be viewed as noise, and the message contained by the non-decoding DU signal is much different. The explicit protocol is described in Section V-A.
In this case, only BS data during odd time slots is relayed by the decoding DU, but D2D data exchange can occur bidirectionally during even time slots.

- Case III: (*Cellular mode*) In this case, the exchanging D2D pair is not able to decode the CU signals. The entire system then degrades into the conventional cellular mode. Thus, we omit the details.

In Fig. 1, the ICI arises since the links from the two senders (BS and D_α) are non-orthogonal. Based on the orthogonality of the in-phase and the quadrature components of a complex constellation, Sun *et al*. [30] exploited signal space diversity (SSD) to separate the two links. Their work motivates us to design the HCFNC (Theorem 1) to mitigate the ICI in D2D.

III. Case I: Successive Spectrum Sharing

In this section, we describe and analyze SSS (Case I) in detail, which can be easily adopted to Case II (Section V) as well. Concurrent transmissions create co-channel interference to CUs and DUs. Thus, to prioritize interference-free transmission and diversity order for the CUs, we propose HCFNC (Theorem 1) and design precoding to match the received signals according to Theorem 1.

Theorem 1. *Considering vectors* $\boldsymbol{w} = \frac{1}{\sqrt{2}}[1, -j]^T$ *and* $\boldsymbol{r} = [r_1, r_2]^T$*, and* $y = \boldsymbol{w}^T\boldsymbol{r} = \frac{1}{\sqrt{2}}(r_1 - jr_2)$*, we have two rules to extract* r_1 *and* r_2 *from* y*.*

Rule-1: If $r_1, r_2 \in \mathbb{R}$*, they can be extracted from* y *using:*

$$r_1 = \sqrt{2}\Re\{y\}, r_2 = -\sqrt{2}\Im\{y\}. \tag{1}$$

Rule-2: If $r_1, r_2 \in \mathbb{C}$*, they can be extracted from* y *using maximum likelihood (ML) detection:*

$$(r_1, r_2) = \arg\min_{r_i \in \mathbb{C}} \parallel y - \frac{1}{\sqrt{2}}(r_1 - jr_2) \parallel . \tag{2}$$

Proof: Eq. (1) can be intuitively derived from the signal space of y. To derive (2), complex field network coding [37], [38] technique is needed. Note that $\boldsymbol{w}$ is taken from the row of the Vandermonde matrix $\begin{bmatrix} 1 & \delta_1 \\ 1 & \delta_2 \end{bmatrix}$, where $\{\delta_u\}_{u=1}^2 = e^{j\pi(4u-1)/4}$. According to [37], the design of $\boldsymbol{w}$ satisfies: $\boldsymbol{w}^T\boldsymbol{r} \neq \boldsymbol{w}^T\widetilde{\boldsymbol{r}}$ if $\boldsymbol{r} \neq \widetilde{\boldsymbol{r}}$, which allows simultaneous transmissions from multiple sources. Then, complex field network coding can be adopted to make it possible that the sources broadcast different symbols in the same time slot and on the same frequency [38]. Finally, as in [37], [38], ML expression (2) can be used to detect r_1 and r_2. ■

Moreover, Equ. (1) from Theorem 1 demands successful demodulation of complex signals only based on their real or the imaginary component. According to [30] signal constellation must be rotated before transmission. Specifically, if u is a complex constellation point from an M-ary alphabet χ, the transmitted symbol is $x = ue^{j\phi}$, where ϕ is chosen to ensure that no two rotated symbols have the same coordinates. That is, for any $p \neq q$,

$$\Re\{x^p\} \neq \Re\{x^q\}, \Im\{x^p\} \neq \Im\{x^q\}, \forall x^p, x^q \in e^{j\phi}\chi. \tag{3}$$

Therefore, prior to the transmission in Case I and II, every constellation symbol is rotated by the angle ϕ chosen from [30]. The transmit symbols $s_B^{(n)}$, $s_\alpha^{(n)}$ and $s_\beta^{(n)}$ are constellation rotated before precoding, and the symbol power satisfies $\mathbb{E}\{|\Re\{s_k^{(n)}\}|^2\} = 1$ $(k \in \{B, \alpha\})$. After the constellation rotation, the transmit symbols in Case I are then precoded based on the phase of related channel fading to match the forms in Theorem 1, which are given by

$$x_B^{(n)} = \Re\{s_B^{(n)}\}e^{-\angle h_C}, \tag{4}$$

$$x_\alpha^{(n)} = \frac{1}{\sqrt{2}}\left(\Re\{s_B^{(n-1)}\} - j\Re\{s_\alpha^{(n)}\}\right)e^{-\angle h_{C\alpha}}, \tag{5}$$

where $1 \leq n \leq L+1$ and $s_B^{(0)} = s_B^{(L+1)} = s_\alpha^{(1)} = 0$. The average power of transmitted symbol during each symbol period is normalized to unity.

In detail, the BS encodes s_B^n by (4) and broadcasts $x_B^{(n)}$ with power P_B. D_α decodes $s_B^{(n-1)}$ received at $(n-1)$-th time slot, and then generates $x_\alpha^{(n)}$ by combining $s_B^{(n-1)}$ with its own symbol $s_\alpha^{(n)}$. D_α broadcasts $x_\alpha^{(n)}$ with power $P_D = \eta P_B$, where η is the power scale coefficient.

Denoting the signals received by CU and D_β as $y_C^{(n)}$ and $y_\beta^{(n)}$, we have

$$y_C^{(n)} = h_C\sqrt{P_B}x_B^{(n)} + h_{C\alpha}\sqrt{P_D}x_\alpha^{(n)} + N_C^{(n)}, \tag{6}$$

$$y_\beta^{(n)} = h_{B\beta}\sqrt{P_B}x_B^{(n)} + h_D\sqrt{P_D}x_\alpha^{(n)} + N_\beta^{(n)}, \tag{7}$$

where $N_C^{(n)}$ and $N_\beta^{(n)}$ denote the noise at CU and D_β respectively. Considering the symbols (4) and (5), we can simplify (6) and (7) as

$$y_C^{(n)} = \frac{1}{\sqrt{2}}\left(r_{1,C}^{(n)} - jr_{2,C}^{(n)}\right), \tag{8}$$

$$y_\beta^{(n)} = \frac{1}{\sqrt{2}}\left(r_{1,\beta}^{(n)} - jr_{2,\beta}^{(n)}\right) + N_\beta^{(n)}, \tag{9}$$

where $r_{1,C}^{(n)}$ and $r_{2,C}^{(n)}$ are real values given by

$$r_{1,C}^{(n)} = |h_C|\sqrt{2P_B}\Re\{s_B^{(n)}\} + |h_{C\alpha}|\sqrt{P_D}\Re\{s_B^{(n-1)}\} + \sqrt{2}\Re\{N_C^{(n)}\}, \tag{10}$$

$$r_{2,C}^{(n)} = |h_{C\alpha}|\sqrt{P_D}\Re\{s_\alpha^{(n)}\} - \sqrt{2}\Im\{N_C^{(n)}\}, \tag{11}$$

and $r_{1,\beta}^{(n)}$ and $r_{2,\beta}^{(n)}$ are complex values given by

$$r_{1,\beta}^{(n)} = \widetilde{h}_{B\beta}\sqrt{2P_B}\Re\{s_B^{(n)}\} + \widetilde{h}_D\sqrt{P_D}\Re\{s_B^{(n-1)}\}, \tag{12}$$

$$r_{2,\beta}^{(n)} = \widetilde{h}_D\sqrt{P_D}\Re\{s_\alpha^{(n)}\}, \tag{13}$$

with $\widetilde{h}_{B\beta} = h_{B\beta}e^{-\angle h_C\alpha}$ and $\widetilde{h}_D = h_D e^{-\angle h_C\alpha}$.

Based on HCFNC theorem, s_B and s_α can be decoded from the composite signals.

A. Protocol

- Time slot 1: the BS broadcasts its precoded data $x_B^{(1)} = f_1(s_B^{(1)})$ to the DUs and C_2.
- Time slot 2: the BS transmits precoded signal $x_B^{(2)} = f_1(s_B^{(2)})$ as (4); D_1 applies the precoding in (5) and transmits the composite signal $x_1^{(2)} = g_1(s_B^{(1)}, s_1^{(2)})$; C_2 first obtains $\boldsymbol{r}_{1,C}(2)$ by Theorem 1, and then detects $s_B^{(2)}$ from $\boldsymbol{r}_{1,C}(2)$ by space-time processing (16); D_2 first obtains $r_{1,\beta}^{(2)}$ and $r_{2,\beta}^{(2)}$ by Theorem 1, and then detects $s_B^{(2)}$ and $s_1^{(2)}$ by successive interference cancellation (SIC) technique (Section III-C).
- Time slot 3: the BS transmits precoded signal $x_B^{(3)} = f_1(s_B^{(3)})$ as (4); D_2 applies the precoding in (5) and

transmits the composite signal $x_2^{(3)} = g_1(s_B^{(2)}, s_2^{(3)})$; D_1 first obtains $r_{1,\beta}^{(3)}$ and $r_{2,\beta}^{(3)}$ by Theorem 1, and then detects $s_B^{(3)}$ and $s_2^{(3)}$ by SIC technique (Section III-C).

- The progress of time slot 2 and time slot 3 repeats alternatively until time slot L.
- Time slot $L+1$: D_α applies the precoding in (5) and transmits the signal $x_\alpha^{(L+1)} = g_1(s_B^{(L)}, s_\alpha^{(L+1)})$; C_2 first obtains $\boldsymbol{r}_{1,C}(L+1)$ by Theorem 1, and then detects $s_B^{(L)}, s_B^{(L-1)}, \cdots, s_B^{(1)}$ from $\boldsymbol{r}_{1,C}(L+1)$ by space-time processing (17); D_β first obtains $r_{2,\beta}^{(L+1)}$ by Theorem 1, and then detects $s_\alpha^{(L+1)}$ by SIC technique (Section III-C).

Note that at time slot $L+1$, a better detection can be achieved by "maximum ratio combining" (MRC) after obtaining $\boldsymbol{r}^f$ and $\boldsymbol{r}^b$. Thus, by exploiting the special signal space structure (Theorem 1), DUs and CUs can decode the cellular data and D2D data.

B. Space-Time Processing at CU

From Rule-1 of Theorem 1, $r_{1,C}^{(n)}$ and $r_{2,C}^{(n)}$ in (8) can be separated using (1), because co-channel interference terms and CU data to DU are readily aligned with the imaginary and real parts of $y_C^{(n)}$ respectively. After retrieving the real part $r_{1,C}^{(n)}$, we focus on the decoding. At the DU, all the cellular data values in $L+1$ time slots are vectorized as

$$\boldsymbol{r}_{1,C} = \mathbf{H}\boldsymbol{s}_B + \boldsymbol{N}_C, \tag{14}$$

where $\boldsymbol{s}_B = \Re\left\{[s_B^{(1)}, s_B^{(2)}, \cdots, s_B^{(L)}]^T\right\}$. The vector $\boldsymbol{N}_C$ is the equivalent noise, i.e., $\boldsymbol{N}_C = \sqrt{2}\Re\left\{[N_C^{(1)}, N_C^{(2)}, \cdots, N_C^{(L+1)}]^T\right\}$. $\mathbf{H}$ is the equivalent MIMO channel matrix of size $(L+1)\times L$,

$$\mathbf{H} = \begin{bmatrix} C_B & 0 & \cdots & 0 & 0 \\ C_1 & C_B & \ddots & 0 & 0 \\ 0 & C_2 & \ddots & 0 & 0 \\ \vdots & \vdots & \ddots & \vdots & \vdots \\ 0 & 0 & \cdots & C_1 & C_B \\ 0 & 0 & \cdots & 0 & C_2 \end{bmatrix}, \tag{15}$$

where $C_B = \sqrt{2P_B}|h_C|$, $C_1 = \sqrt{P_D}|h_{C1}|$, $C_2 = \sqrt{P_D}|h_{C2}|$ and L is assumed to be even.

Only one non-zero entry exists in the first and last rows of $\mathbf{H}$ respectively, which manifests that $s_B^{(1)}$ and $s_B^{(L)}$ can be estimated directly from the observations at the first and last time slots. Then, based on the special structure[2] of $\mathbf{H}$, inter-symbol interference (ISI) terms $C_B s_B^{(1)}$ (forward direction) and $C_1 s_B^{(L)}$ (backward direction) can be reconstructed and subtracted from observations at the 2-th and $(L-1)$-th time slots respectively. Following this same progress, the decoder is able to subtract the reconstructed ISI from the observation at each time slot in sequence. Accordingly, this forward and backward estimation method [33] outputs $\boldsymbol{s}^f$ and $\boldsymbol{s}^b$, which are the hard decisions of $\boldsymbol{r}^f$ and $\boldsymbol{r}^b$ respectively. $\boldsymbol{r}^f(n)$ and $\boldsymbol{r}^b(n)$ are given by

$$\boldsymbol{r}^f(n) = \begin{cases} \boldsymbol{r}_{1,C}(n), & n=1, \\ \boldsymbol{r}_{1,C}(n) - \boldsymbol{s}^f(n-1)\mathbf{H}(n,n-1), & 1<n\le L, \end{cases} \tag{16}$$

$$\boldsymbol{r}^b(n) = \begin{cases} \boldsymbol{r}_{1,C}(n+1), & n=L, \\ \boldsymbol{r}_{1,C}(n+1) - \boldsymbol{s}^b(n+1)\mathbf{H}(n+1,n+1), & 1\le n<L. \end{cases} \tag{17}$$

[2]For more general $\mathbf{H}$, we can apply the Babai estimator [39] or sphere decoding [40].

Either the forward or backward estimations can be used in data detection. A better detection can be achieved by MRC $\boldsymbol{r}^f$ and $\boldsymbol{r}^b$ as

$$\boldsymbol{r}^{\mathrm{MRC}}(n) = \mathbf{H}(n,n)\boldsymbol{r}^f(n) + \mathbf{H}(n+1,n)\boldsymbol{r}^b(n),\ n=1,\cdots,N, \tag{18}$$

with the final data detection being the hard decision of $\boldsymbol{r}^{\mathrm{MRC}}$.

In practice, hard decision errors exist in forward and backward estimation, leading to a performance gap with ideal decoding. The evaluation of the performance gap is beyond the scope of this paper and may be considered in future work.

C. SIC Detection at DU

From Rule-2 of Theorem 1, $r_{1,\beta}$ and $r_{2,\beta}$ in (9) can be separated using HCFNC. Since symbol errors may be caused by random noise $N_\beta^{(n)}$, the symbol error probability (SEP) will be given in Section IV-B. Here, we focus on the decoding process after separating $r_{1,\beta}$ and $r_{2,\beta}$, i.e. extracting the expected signals $s_B^{(n)}$ and $s_\alpha^{(n)}$.

It is easy to decode $s_\alpha^{(n)}$ from (13). To decode $s_B^{(n)}$ from (12), we use target rate R_D^{tar} to implement the SIC detection. Define

$$\begin{aligned} g_{\max} &= \arg\max\{2P_B|\widetilde{h}_{B\beta}|^2, P_D|\widetilde{h}_D|^2\} \\ &= \arg\max\{2P_B|h_{B\beta}|^2, P_D|h_D|^2\}, \end{aligned} \tag{19}$$

$$\begin{aligned} g_{\min} &= \arg\min\{2P_B|\widetilde{h}_{B\beta}|^2, P_D|\widetilde{h}_D|^2\} \\ &= \arg\min\{2P_B|h_{B\beta}|^2, P_D|h_D|^2\}, \end{aligned} \tag{20}$$

and $R_D^{\mathrm{SIC}} = \log_2\left(1+\frac{g_{\max}}{g_{\min}}\right)$. We have the following criterion

$$R_D^{\mathrm{SIC}} \ge R_D^{tar}, \tag{21}$$

which allows the SIC to process successfully. The stronger signal can be successfully decoded by treating the other as noise. After that, the stronger signal can be reconstructed and canceled, which helps to decode the weaker signal.

D. Feasible Region for D2D Power Scale Coefficient η

To implement the D2D relaying process successfully, the transmit power of DU is constrained by $P_D = \eta P_B$ and (21). We determine the feasible region for η in Lemma 1.

Lemma 1.

$$\eta \in \begin{cases} \mathbb{R}^+, & 0 < R_D^{tar} \le 1, \\ (0, \frac{G}{2^{R_D^{tar}}-1}] \bigcup [(2^{R_D^{tar}}-1)G, \infty), & R_D^{tar} > 1, \end{cases} \tag{22}$$

where $G = \frac{2|h_{S\beta}|^2}{|h_D|^2}$.

Proof: Please see Appendix I. ■

Remark 1. *If the target decoding rate R_D^{tar} is smaller than 1, there is no limit for P_D considering SIC. Whereas, in practice, the transmit power of D2D user can hardly be larger than that of BS, i.e., $\eta = \frac{P_D}{P_B} < 1$. On the other hand, $\frac{G}{2} = \frac{|h_{B\beta}|^2}{|h_D|^2} < 1$ holds due to the proximity for D2D user pairs. Based on the two facts, the choice for η in practice can be $\eta \in (0,1)$ $(R_D^{tar} \le 1)$ or $\eta \in (0,1] \bigcap (0, \frac{G}{2^{R_D^{tar}}-1}] \bigcup [(2^{R_D^{tar}}-1)G, \infty)$ $(R_D^{tar} > 1)$.*

IV. Performance Results for Case I

A. Diversity-Multiplexing Tradeoff Analysis for CU

Since in Case I the two DUs can correctly decode the original BS data in the first relaying phase, we only focus on the mutual information in the second relaying phase. This can be expressed using the equivalent MISO channel model in (14) as

$$I(\boldsymbol{s}_B;\boldsymbol{y}_C) = \log_2\left(\det\left(\mathbf{I}_{L+1}+\mathbf{H}\mathbf{R}_{\boldsymbol{s}_B}\mathbf{H}^{\mathrm{H}}\mathbf{R}_{\boldsymbol{N}_C}^{-1}\right)\right) \quad (23)$$

$$= \log_2\left(\det\left(\mathbf{I}_{L+1}+\frac{1}{\sigma^2}\mathbf{H}\mathbf{H}^{\mathrm{H}}\right)\right), \quad (24)$$

where $\mathbf{R}_{\boldsymbol{s}_B}=\mathbb{E}\{\boldsymbol{s}_B\boldsymbol{s}_B^{\mathrm{H}}\}=\mathbf{I}_L$ and $\mathbf{R}_{\boldsymbol{N}_C}=\mathbb{E}\{\boldsymbol{N}_C\boldsymbol{N}_C^{\mathrm{H}}\}=\sigma^2\mathbf{I}_{L+1}$. Thus, the outage probability of CU is given by

$$P_{out}^{CU} = Pr\left\{I(\boldsymbol{s}_B;\boldsymbol{y}_C)<(L+1)R\right\}$$
$$= Pr\left\{\log_2\left(\det\left(\mathbf{I}_{L+1}+\frac{1}{\sigma^2}\mathbf{H}\mathbf{H}^{\mathrm{H}}\right)\right)<(L+1)R\right\}. \quad (25)$$

The factor $L+1$ is the number of $L+1$ time slots required to transmit L symbols [41].

1) DMT Lower Bound: $\mathbf{H}$ is an $(L+1)\times L$ bi-diagonal matrix and can be shown to be in the following form:

$$\mathbf{H} = \begin{bmatrix} C_B\mathbf{I}_L \\ \boldsymbol{0}^{\mathrm{T}} \end{bmatrix} + \begin{bmatrix} \boldsymbol{0}^{\mathrm{T}} \\ \mathrm{diag}(\boldsymbol{C}) \end{bmatrix}, \quad (26)$$

where $\boldsymbol{C}=[C_1,C_2,\cdots,C_1,C_2]^{\mathrm{T}}$ and $\boldsymbol{0}=[0,0,\cdots,0]^{\mathrm{T}}$ are both L-dimensional vectors. By using the Lemma 3.1 in [41] and observing the structure of $\mathbf{H}$ in (15), we have

$$\det\left(\mathbf{I}_{L+1}+\frac{1}{\sigma^2}\mathbf{H}\mathbf{H}^{\mathrm{H}}\right)$$
$$\geq \left(\frac{1}{\sigma^2}|C_B|^2\right)^L + \left(1+\frac{1}{\sigma^2}|C_1|^2\right)^{\frac{L}{2}}\left(1+\frac{1}{\sigma^2}|C_2|^2\right)^{\frac{L}{2}}$$
$$\doteq \mathrm{SINR}^L\left(\left(2|h_C|^2\right)^L+\left(\eta^2|h_{C1}|^2|h_{C2}|^2\right)^{\frac{L}{2}}\right), \quad (27)$$

where the dot equal operator $\doteq$ denotes asymptotic equality in the high SINR regime, $\mathrm{SINR}=\frac{P_B}{\sigma^2}$ and $\eta=\frac{P_D}{P_B}$. From (25) and (27), we obtain

$$\mathrm{SINR}^{-d(r)} \doteq P_{out}^{CU} \leq P_r\left\{\log_2\left(\mathrm{SINR}^L\left(\left(2|h_C|^2\right)^L + \left(\eta^2|h_{C1}|^2|h_{C2}|^2\right)^{\frac{L}{2}}\right)\right)<(L+1)R\right\}$$
$$\doteq \mathrm{SINR}^{-\underline{d(r)}}, \quad (28)$$

where $R=r\log_2(\mathrm{SINR})$ and $\underline{d(r)}$ is the lower bound.

The outage events at high SINR are dominated by

$$\begin{cases} \log_2\left(\mathrm{SINR}^L\left(2|h_C|^2\right)^L\right)<(L+1)R \\ \log_2\left(\mathrm{SINR}^L\left(\eta^2|h_{C1}|^2|h_{C2}|^2\right)^{\frac{L}{2}}\right)<(L+1)R \end{cases}, \quad (29)$$

which can be simplified as

$$\begin{cases} |h_C|^2 < 2^{-1}\mathrm{SINR}^{(\frac{L+1}{L}r-1)} \\ |h_{C1}|^2\cdot|h_{C2}|^2 < \eta^{-1}\mathrm{SINR}^{2(\frac{L+1}{L}r-1)} \end{cases}. \quad (30)$$

By using (30) and the exponential order of h_k, $k\in\{C,C1,C2\}$, i.e., $v_k=-\lim_{\mathrm{SINR}\to\infty}\frac{\log_2(|h_k|^2)}{\log_2(\mathrm{SINR})}$, we can rewrite the outage events in the high SINR regime as

$$O^+ = \{(v_C,v_{C1},v_{C2})\in\mathbb{R}^{3+} \left| \begin{matrix}(1-v_C)^+<\frac{L+1}{L}r, \\ (2-v_{C1}-v_{C2})^+<\frac{L+1}{L}2r\end{matrix}\right\}, \quad (31)$$

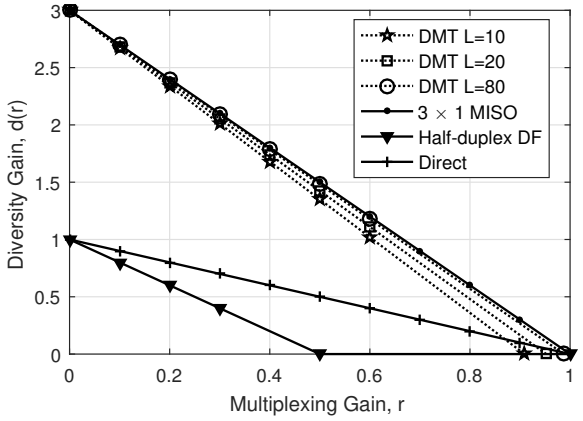

Fig. 2. DMT performance for CU in Case I. Half-duplex DF relaying refers to [42], and 'direct' means direct transmission without relaying.

By using (31) and according to [41], the DMT lower bound can be expressed as

$$\underline{d_o(r)} = \inf_{O^+}(v_C+v_{C1}+v_{C2}) = 3\left(1-\frac{L+1}{L}r\right)^+, \quad (32)$$

where the notion inf stands for the infimum of a set.

2) DMT Upper Bound: This is actually a two-relay diversity protocol, and the DMT is upper bounded by the 3×1 MISO DMT [41] given by

$$\overline{d_o(r)} = 3\left(1-\frac{L+1}{L}r\right)^+. \quad (33)$$

Then, the DMT in closed-form is given as

$$d_o(r) = \overline{d_o(r)} = \underline{d_o(r)} = 3\left(1-\frac{L+1}{L}r\right)^+. \quad (34)$$

Remark 2. *The closed-form expression of the achievable DMT (34) indicates that the proposed D2D aided two-hop cellular transmission achieves a multiplexing gain of $\frac{L}{L+1}$, which can be approximated as 1 (full-duplex). On the other hand, the cellular transmission achieves a full diversity of 3 and approaches the 3×1 MISO DMT. The numerical results in Fig. 2 verify that D2D user's DMT approaches 3×1 MISO DMT when L is large. Compared with direct transmission and half-duplex relaying, DUs' special assistance in SSS scheme helps the cellular system maintaining the multiplexing gain and achieving a higher diversity order of three instead of one.*

B. DU's Symbol Error Probability after HCFNC

In this section we consider the DU SEP after HCFNC, which is affected by the decoding (Theorem 1) and noise.

To analyze the SEP for CU, we rewrite (9) in the standard AWGN channel form as

$$y_\beta^{(n)} = X^{(n)} + N_\beta^{(n)}, \quad (35)$$

where $X^{(n)}=\frac{1}{\sqrt{2}}\left(u_1^{(n)}-ju_2^{(n)}\right)$, $X^{(n)}\in A_X$, $u_1^{(n)}=\widetilde{h}_{B\beta}\sqrt{2P_B}\Re\{s_B^{(n)}\}+\widetilde{h}_D\sqrt{P_D}\Re\{s_B^{(n-1)}\}$, $u_2^{(n)}=\widetilde{h}_D\sqrt{P_D}\Re\{s_\alpha^{(n)}\}$ and $u_1^{(n)},u_2^{(n)}\in A_u$. Assuming $X_a^{(n)}$ and $X_b^{(n)}$ are two

realizations for $X^{(n)}$, the SEP of $X^{(n)}$ is given by

$$P_e\{X^{(n)}\} = \sum_{a=1}^{N_n} P_r\{X_a^{(n)}\} \sum_{\substack{b=1 \\ X_b^{(n)} \neq X_a^{(n)}}}^{N_n} P_r\{X_a^{(n)} \to X_b^{(n)}\}, \quad (36)$$

where $N_n = |A_X|$. However, the incorrect detection of X does not represent the error of two symbols $(u_1^{(n)}, u_2^{(n)})$, because the number of symbols failed to be recovered is unknown. The probability $P_{e-k}^{(n)}$ $(k = 1, 2)$, denoting k of two symbols $(u_1^{(n)}, u_2^{(n)})$ failed to be recovered, is given by

$$P_{e-k}^{(n)} = \sum_{a=1}^{N_n} P_r\{X_a^{(n)}\} \sum_{b=1}^{N_n} P_r\{X_a^{(n)} \to X_b^{(n)} \mid \|\boldsymbol{u}_a^{(n)} - \boldsymbol{u}_b^{(n)}\|_0 = k\}, \quad (37)$$

where $X_a^{(n)} = \boldsymbol{w}^{\mathrm{T}}\boldsymbol{u}_a^{(n)}$, $X_b^{(n)} = \boldsymbol{w}^{\mathrm{T}}\boldsymbol{u}_b^{(n)}$ and $\boldsymbol{w}$ is given in Theorem 1. $\boldsymbol{u}_a^{(n)}$ and $\boldsymbol{u}_b^{(n)}$ are two realizations for $\boldsymbol{u}^{(n)} = [u_1^{(n)}, u_2^{(n)}]^{\mathrm{T}}$. $\|\boldsymbol{u}_a^{(n)} - \boldsymbol{u}_b^{(n)}\|_0$ indicates the zero-norm which denotes the number of nonzero elements of $(\boldsymbol{u}_a^{(n)} - \boldsymbol{u}_b^{(n)})$. Hence, the average SEP for each symbol in $(u_1^{(n)}, u_2^{(n)})$ can be expressed as

$$P_e^{(n)} = \frac{1}{N_s} \sum_{k=1}^{N_s} k \times P_{e-k}^{(n)}, \quad (38)$$

where $N_s = 2$ is the number of symbols coded in $X^{(n)}$. We assume the uniform distribution of $X^{(n)}$ due to one-to-one mapping between $X^{(n)}$ and $\boldsymbol{u}^{(n)}$ [37], i.e. $P_r\{X_a^{(n)}\} = 1/|A_X|$. For any given constellation in (37), the SEP in AWGN channel can be estimated by the union bound [39], [43]:

$$P_{e-k}^{(n)} \leq \frac{1}{|A_X|} \sum_{a=1}^{N_n} \left(\sum_{\substack{b=1 \\ \|\boldsymbol{u}_a^{(n)} - \boldsymbol{u}_b^{(n)}\|_0 = k}}^{N_n} Q\left(\frac{d_{ab}^{X^{(n)}}}{2\sqrt{\sigma^2}}\right) \right), \quad (39)$$

where $d_{ab}^{X^{(n)}}$ denotes the Euclidean distance between $X_a^{(n)}$ and $X_b^{(n)}$ in the constellation for $X^{(n)}$, and $\|\boldsymbol{u}_a^{(n)} - \boldsymbol{u}_b^{(n)}\|_0 = k$ indicates the zero-norm denoting the number of nonzero elements of $(\boldsymbol{u}_a^{(n)} - \boldsymbol{u}_b^{(n)})$ is k. The SEP (38) is upper bounded by

$$P_e^{(n)} \leq \frac{1}{2N_n} \sum_{k=1}^{2} k \sum_{a=1}^{N_n} \left(\sum_{\substack{b=1 \\ \|\boldsymbol{u}_a^{(n)} - \boldsymbol{u}_b^{(n)}\|_0 = k}}^{N_n} Q\left(\frac{d_{ab}^{X^{(n)}}}{2\sqrt{\sigma^2}}\right) \right). \quad (40)$$

C. Lower Bound for DU's Throughput with HCFNC

To extract DU own symbol contained in $r_{2,\beta}^{(n)}$, HCFNC is needed to separate the cooperative symbol $r_{1,\beta}^{(n)}$ and non-cooperative symbol $r_{2,\beta}^{(n)}$. The throughput $T^{(n)}$ of the D2D link, defined as the average number of successfully transmitted symbols within one time slot [37], is affected by the SEP of HCFNC.

$$T^{(n)} = \begin{cases} 0, & n = 1 \\ 1 - P_e^{(n)}, & 2 \leq n \leq L+1 \end{cases} \quad \text{(sym/TS)}. \quad (41)$$

The average throughput of D2D link over $L+1$ time slots can be given by

$$T_D = \frac{1}{L+1} \sum_{n=1}^{L+1} T^{(n)} \quad (42)$$

$$\geq \frac{1}{L+1} \sum_{n=2}^{L+1} \left(1 - \frac{1}{2N_n} \sum_{k=1}^{2} k \sum_{a=1}^{N_n} \left(\sum_{\substack{b=1 \\ \|\boldsymbol{u}_a^{(n)} - \boldsymbol{u}_b^{(n)}\|_0 = k}}^{N_n} Q\left(\frac{d_{ab}^{X^{(n)}}}{2\sqrt{\sigma^2}}\right) \right) \right). \quad (43)$$

Thus, T_D is lower bounded by (43), which approximates the practical throughput, especially in high SINR regime. When SINR approaches to infinity (i.e. $\sigma \to 0$), the lower bound for throughput is

$$\underline{T_D} = \lim_{\sigma \to 0} \frac{1}{L+1} \sum_{n=2}^{L+1} \left(1 - \frac{1}{2N_n} \sum_{k=1}^{2} k \sum_{a=1}^{N_n} \left(\sum_{\substack{b=1 \\ \|\boldsymbol{u}_a^{(n)} - \boldsymbol{u}_b^{(n)}\|_0 = k}}^{N_n} Q\left(\frac{d_{ab}^{X^{(n)}}}{2\sqrt{\sigma^2}}\right) \right) \right)$$

$$= \frac{L}{L+1}. \quad (44)$$

Note that the lower bound for D2D throughput approaches 1 as $L \to \infty$.

Remark 3. *The lower bound for the D2D average throughput given in (43) can be approximated as $\frac{L}{L+1}$ in high SINR regime. Thus, when the channel condition is good and L is large enough, the D2D throughput is 1 sym/TS. Then, DU can access cellular spectrum in each time slot to exchange its data for local services, which infers that D2D system gains full spectrum access opportunity. The numerical results in Fig. 3 verify that: 1) the derived lower bound is very close to simulation value; 2) the throughput is very near to 1 sym/TS when SINR (tranmit power) is larger than 25 dB.*

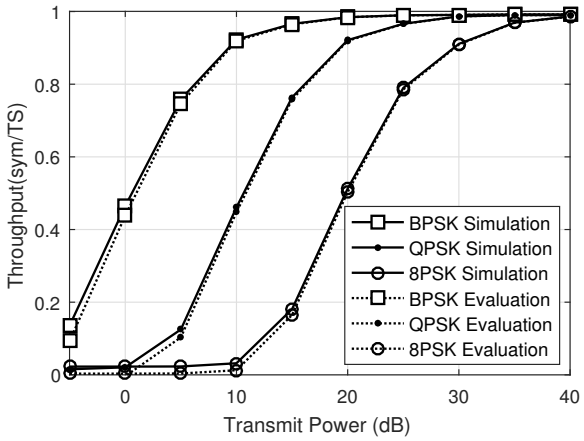

Fig. 3. The average throughput for DU in Case I. Simulation is based on these parameters: frame length $L + 1 = 129$, background AWGN noise variance $\sigma^2 = 1$, Rayleigh fading channel coefficient variance $\sigma_{h_k}^2 = 1$ $(k \in \{C, B1, B2, D, C1, C2\})$, the power scale coefficient $\eta = 0.5$, path loss factor is 3, and distances of DU-DU and CU-DU are set as 0.5 and 1 respectively. Evaluation is based on the lower bound derived in (43).

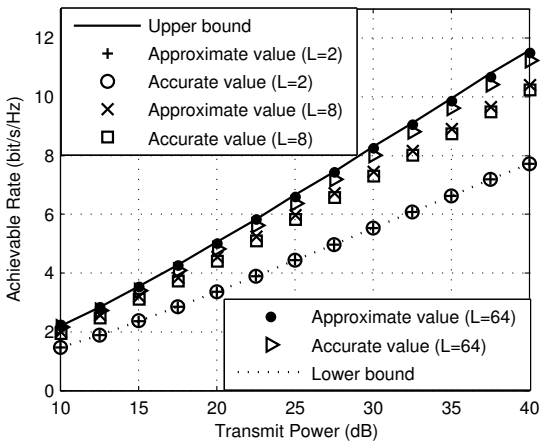

Fig. 4. Achievable rate for CU in Case I. Simulation parameters: background AWGN noise variance $\sigma^2 = 1$, Rayleigh fading channel coefficient variance $\sigma^2_{h_k} = 1$ ($k \in \{C, B1, B2, D, C1, C2\}$), the power scale coefficient $\eta = 0.5$, path loss factor is 3, and distances of DU-DU, DU-CU and BS-CU are set as 1, 1 and $\sqrt{3}$ respectively.

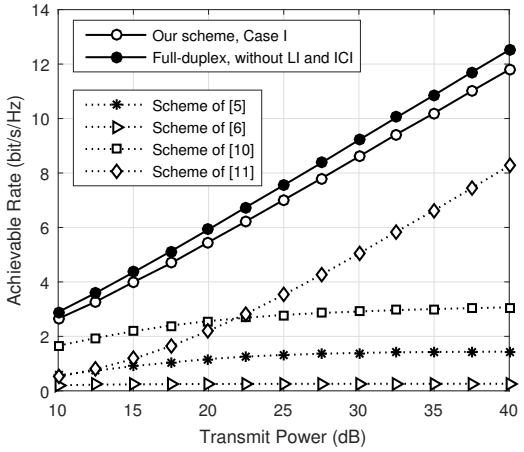

Fig. 5. Achievable rate for CU in Case I. The ideal achievable rate for full-duplex relaying ignoring LI and ICI is an upper bound for all schemes. Simulation parameters: frame length $L + 1 = 33$ and other parameters are the same with Fig. 4. For schemes using superposition coding, the power split factors at DUs are fixed at 0.8 for fair comparison.

D. Achievable Rate for the CU Channel

Similar to [12], the achievable rate for (24) can be calculated as

$$R_C = \frac{1}{L+1}\log_2\left(\det\left(\boldsymbol{I}_{L+1} + \mathbf{H}_c\mathbf{H}_c^{\mathrm{H}}\right)\right) \text{ bit/s/Hz}, \tag{45}$$

where $\mathbf{H}_c = \frac{1}{\sigma}\mathbf{H}$. To simplify the evaluation of the determinants (45), The normalized equivalent MIMO channel in (45) can be approximated by

$$\mathbf{H}_c \approx \begin{bmatrix} \mathbf{H}_0 & & \\ & \ddots & \\ & & \mathbf{H}_0 \end{bmatrix}, \ \mathbf{H}_0 = \frac{1}{\sigma}\begin{bmatrix} C_B & 0 \\ C_1 & C_B \\ 0 & C_2 \end{bmatrix}. \tag{46}$$

The determinant of the tridiagonal martix is evaluated as [12]

$$\det\left(\boldsymbol{I}_{L+1} + \mathbf{H}_c\mathbf{H}_c^{\mathrm{H}}\right) \approx \left(\det(\boldsymbol{I}_3 + \mathbf{H}_0\mathbf{H}_0^{\mathrm{H}})\right)^{\frac{L}{2}} = |B|^{\frac{L}{2}}, \tag{47}$$

where $|B| = 1 + \frac{4P_B g_c}{\sigma^2} + \frac{P_D g_{c1}}{\sigma^2} + \frac{P_D g_{c2}}{\sigma^2} + \frac{4P_B^2 g_c}{\sigma^4} + \frac{P_D^2 g_{c1} g_{c2}}{\sigma^4} + \frac{2P_B P_D g_c g_{c1}}{\sigma^4}$. Thus, the achievable rate can be approximated by

$$R_C \approx R'_C = \frac{L\log_2|B|}{2(L+1)} = \frac{1}{2}\log_2|B| - \frac{1}{2(L+1)}\Delta R, \tag{48}$$

where $\Delta R = \log_2|B|$. It can be concluded from (48) that bounds for R'_c exist, because $L \in (2, \infty)$.

$$\frac{1}{3}\log_2|B| < R'_c < \frac{1}{2}\log_2|B|. \tag{49}$$

Remark 4. *The numerical results (Fig. 4) verify that: 1) the derived approximated rate is very close to accurate value; 2) if the frame length is more than 64, we can use the upper bound to estimate CU rate, which is useful in practical applications.*

The numerical results (Fig. 5) compare our scheme with some existing CSS schemes. The schemes of [7], [8], [12] use superposition coding to combine DU data with the relaying data for CU. 1) In schemes [7], [8], [12], the intended data for cellular user is always interfered by DU signal (ICI), which results in a SINR floor as transmit power increases. The ICI limits CU performance especially at high SINR regime. Thus, our scheme outperforms these schemes because HCFNC technique creates interference-free channel for the priority user (CU). 2) Our scheme outperforms the scheme in [13], because direct link can be utilized in our scheme to enlarge the capacity of equivalent MIMO channel while the ANC relaying protocol in [13] can not. 3) The data rate for CU in our scheme is very close to the full-duplex relaying in this scenario, which is considered ideally without any interferences. Thus, full-duplex multiplexing gain can be achieved if L is chosen large enough and CSI is accurate to support HCFNC technique.

E. Achievable Rate for CU Channel with PEE

HCFNC is implemented via precoding at the transmitter. The precoding processes (4) and (5) require channel phase estimations for h_C and $h_{C\alpha}$. However, nodes may not always acquire perfect CSI due to, for example, channel estimation errors and/or the slack cooperation between DUs and CUs [44]. Specifically, PEE or phase noise in channel estimation greatly affects the signal constellation based approaches [18]. Thus, it is important to characterize the effect of PEE on the achievable rate for the cellular user.

Consider $\Delta\phi_C, \Delta\phi_D \sim N(0, \Delta_P^2)$ [18] and they are PEEs for CU and DU, respectively. Thus, the transmit symbols are given by

$$\widetilde{x}_B^{(n)} = \Re\{s_B^{(n)}\}e^{-(\angle h_C + \Delta\phi_C)}, \tag{50}$$

$$\widetilde{x}_\alpha^{(n)} = \frac{1}{\sqrt{2}}\left(\Re\{s_B^{(n-1)}\} - j\Re\{s_\alpha^{(n)}\}\right)e^{-(\angle h_C\alpha + \Delta\phi_D)}. \tag{51}$$

Thus, we have

$$\widetilde{y}_C^{(n)} = h_C\sqrt{P_B}\widetilde{x}_B^{(n)} + h_{C\alpha}\sqrt{P_D}\widetilde{x}_\alpha^{(n)} + N_C^{(n)}, \tag{52}$$

where $\widetilde{r}_{1,C}^{(n)} = \sqrt{2}\Re\{\widetilde{y}_C^{(n)}\}$, i.e.,

$$\begin{aligned}\widetilde{r}_{1,C}^{(n)} =& |h_C|\sqrt{2P_B}\Re\{s_B^{(n)}\}\cos\Delta\phi_C + |h_{C\alpha}|\sqrt{P_D}\Re\{s_B^{(n-1)}\} \\ &\times\cos\Delta\phi_D + |h_{C\alpha}|\sqrt{P_D}\Re\{S_\alpha^{(n)}\}\sin\Delta\phi_D + \sqrt{2}\Re\{N_C^{(n)}\}.\end{aligned} \tag{53}$$

At DU, all the $\widetilde{r}_{1,C}^{(n)}$ in $L+1$ time slots (a frame) are

$$\widetilde{\boldsymbol{r}}_{1,C} = \widetilde{\mathbf{H}}\boldsymbol{s}_B + \widetilde{\boldsymbol{w}}, \tag{54}$$

where the equivalent interference plus noise vector $\widetilde{\boldsymbol{w}}$ is

$$\widetilde{\mathbf{w}}=\sqrt{P_D}\sin\Delta\phi_D\begin{bmatrix}0\\ |h_{C1}|\Re\{S_1^{(2)}\}\\ |h_{C2}|\Re\{S_2^{(3)}\}\\ \vdots\\ |h_{C2}|\Re\{S_2^{(L+1)}\}\end{bmatrix}+\sqrt{2}\begin{bmatrix}\Re\{N_C^{(1)}\}\\ \Re\{N_C^{(2)}\}\\ \Re\{N_C^{(3)}\}\\ \vdots\\ \Re\{N_C^{(L+1)}\}\end{bmatrix}. \quad (55)$$

$\widetilde{\mathbf{H}}$ is the equivalent MIMO channel with size $(L+1)\times L$,

$$\widetilde{\mathbf{H}}=\begin{bmatrix}\widetilde{C}_B & 0 & \cdots & 0 & 0\\ \widetilde{C}_1 & \widetilde{C}_B & \ddots & 0 & 0\\ 0 & \widetilde{C}_2 & \ddots & 0 & 0\\ \vdots & \vdots & \ddots & \vdots & \vdots\\ 0 & 0 & \cdots & \widetilde{C}_1 & \widetilde{C}_B\\ 0 & 0 & \cdots & 0 & \widetilde{C}_2\end{bmatrix}, \quad (56)$$

where $\widetilde{C}_B=C_B\cos\Delta\phi_C$ and $\widetilde{C}_i=C_i\cos\Delta\phi_D$ $(i\in 1,2)$.

Based on [12], the achievable rate for the case with PEE is

$$\begin{aligned}\widetilde{R}_c&=\frac{1}{L+1}\log_2\left(\det\left(\boldsymbol{I}_{L+1}+\widetilde{\mathbf{H}}^{\mathrm{H}}(\mathbf{R}_{\boldsymbol{w}}^{-\frac{1}{2}})^{\mathrm{H}}\widetilde{\mathbf{H}}\mathbf{R}_{\boldsymbol{w}}^{-\frac{1}{2}}\right)\right)\\&=\frac{1}{L+1}\log_2\left(\det\left(\boldsymbol{I}_{L+1}+\widetilde{\mathbf{H}}_c\widetilde{\mathbf{H}}_c^{\mathrm{H}}\right)\right), \quad (57)\end{aligned}$$

where $R_{\boldsymbol{w}}=\mathbb{E}\{\boldsymbol{w}\boldsymbol{w}^{\mathrm{H}}\}=\mathrm{diag}\{\sigma^2,\lambda_1,\lambda_2,\cdots,\lambda_2\}$, with $\lambda_1=g_{C1}P_D\sin^2\Delta\phi_D+\sigma^2$ and $\lambda_2=g_{C2}P_D\sin^2\Delta\phi_D+\sigma^2$. The normalized equivalent MIMO channel $\widetilde{\mathbf{H}}_c$ is written as

$$\widetilde{\mathbf{H}}_c=\begin{bmatrix}\frac{\widetilde{C}_B}{\sigma} & 0 & \cdots & 0 & 0\\ \frac{\widetilde{C}_1}{\sqrt{\lambda_1}} & \frac{\widetilde{C}_B}{\sqrt{\lambda_1}} & \ddots & 0 & 0\\ 0 & \frac{\widetilde{C}_2}{\sqrt{\lambda_2}} & \ddots & 0 & 0\\ \vdots & \vdots & \ddots & \vdots & \vdots\\ 0 & 0 & \cdot & \frac{\widetilde{C}_1}{\sqrt{\lambda_1}} & \frac{\widetilde{C}_B}{\sqrt{\lambda_1}}\\ 0 & 0 & \cdots & 0 & \frac{\widetilde{C}_2}{\sqrt{\lambda_2}}\end{bmatrix}. \quad (58)$$

Adopting the same procedure in (45)-(48), the approximation of $\widetilde{R}_C$ can be derived as (see Appendix II),

$$\widetilde{R}_C\approx\widetilde{R}'_C=\frac{1}{2}\log_2\left(|B_2|\right)+\frac{1}{L+1}\Delta\widetilde{R}. \quad (59)$$

In (59), $\Delta\widetilde{R}=\log_2\left(|B_1|\cdot|B_2|^{-\frac{3}{2}}\right)$ and

$$|B_1|=1+\frac{\widetilde{C}_1^2}{\lambda_1}+\frac{\widetilde{C}_B^2}{\lambda_1}+\frac{\widetilde{C}_2^2}{\lambda_2}+\frac{\widetilde{C}_1^2\widetilde{C}_2^2}{\lambda_1\lambda_2}+\frac{\widetilde{C}_B^2}{\sigma^2}+\frac{\widetilde{C}_B^4}{\lambda_1\sigma^2}+\frac{\widetilde{C}_2^2\widetilde{C}_B^2}{\lambda_2\sigma^2}, \quad (60)$$

$$|B_2|=1+\frac{\widetilde{C}_1^2}{\lambda_1}+\frac{\widetilde{C}_B^2}{\lambda_1}+\frac{\widetilde{C}_2^2}{\lambda_2}+\frac{\widetilde{C}_1^2\widetilde{C}_2^2}{\lambda_1\lambda_2}+\frac{\widetilde{C}_B^2}{\lambda_2}+\frac{\widetilde{C}_B^4}{\lambda_1\lambda_2}+\frac{\widetilde{C}_2^2\widetilde{C}_B^2}{\lambda_2^2}. \quad (61)$$

As $L\in(2,\infty)$, the bounds for $\widetilde{R}'_C$ exist:

$$\frac{1}{3}\log_2|B_1|<\widetilde{R}'_C<\frac{1}{2}\log_2|B_2|. \quad (62)$$

When L is sufficiently small, $\widetilde{R}'_C$ approaches $\frac{1}{3}\log_2|B_1|$ and is determined by $|B_1|$. When L is sufficiently large, $\widetilde{R}'_C$ approaches $\frac{1}{2}\log_2|B_2|$ and is determined by $|B_2|$.

To evaluate the effect of PEE on achievable rate, we firstly give the following high-SINR expressions: $\lim_{\gamma\to\infty}\frac{\widetilde{C}_i^2}{\lambda_i}=\cot^2\Delta\phi_D$, $\lim_{\gamma\to\infty}\frac{\widetilde{C}_B^2}{\lambda_i}=\frac{2g_C}{\eta g_{Ci}}\frac{\cos^2\Delta\phi_C}{\sin^2\Delta\phi_D}=\frac{b_i}{\sin^2\Delta\phi_D}$ and $\lim_{\gamma\to\infty}\frac{\widetilde{C}_B^2}{\sigma^2}=\infty$ ($\gamma=\frac{P_D}{\sigma^2}$, $\eta=\frac{P_D}{P_B}$ and $i\in\{1,2\}$). Then,

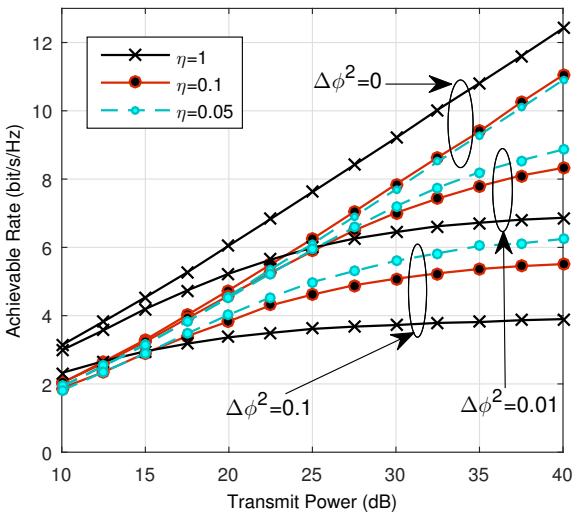

Fig. 6. Achievable rate for CU with PEE in Case I. Different power scale coefficient η and different PEE $\Delta\phi=\Delta\phi_C=\Delta\phi_D$ is chosen to make comparison. Simulation parameters: frame length $L+1=33$, and other parameters are the same with Fig. 4.

we derive that

$$\lim_{\gamma\to\infty}|B_1|=\infty, \quad (63)$$

$$\begin{aligned}\lim_{\gamma\to\infty}|B_2|=&(1+\cot^2\Delta\phi_D)^2+b_2\cot^2\Delta\phi_D\\&+\frac{1}{\sin^2\Delta\phi_D}(b_1+b_2+\frac{b_1b_2}{\sin^2\Delta\phi_D}). \quad (64)\end{aligned}$$

Note that at the high SINR regime, the achievable rate for equivalent MIMO channel is

$$\lim_{\gamma\to\infty}\widetilde{R}'_C=\begin{cases}\infty, & L\to 2,\\ \frac{1}{2}\log_2(A), & L\to\infty,\end{cases} \quad (65)$$

where finite value $A=\lim_{\gamma\to\infty}|B_2|$ is given in (64).

Remark 5. *Observing (55), we note that additional interference is overlaying the background AWGN. This term is weighted by $\sqrt{P_D}$ and PEE component $\sin\Delta\phi_D$, which limits the maximum achievable rate at high SINR. Thus, the channel estimations for DU-CU links, i.e. h_{C1} and h_{C2}, are more important in order to achieve higher D2D aided cellular rate. This can be validated by (64) and (65) that: $\widetilde{R}'_C\to\infty$ as the PEEs of DU-CU links approach zero ($\Delta\phi_D\to 0$).*

Based on (65), in the scenario with small frame length $L\to 2$, the achievable rate can increase infinitely as SINR increases. Whereas, direct cellular link in the first time slot plays the most important part in equivalent MIMO channel capacity, and the rates of the D2D aided cellular links are still limited by PEE induced interference. According to Remark 2, to achieve full multiplexing gain, large frame length ($L\to+\infty$) must be chosen in system design. Thus, the scenario with large frame length L is approval in practice.

In any case, the achievable rates for D2D aided cellular links are limited by PEE induced interference. And the analysis can be verified by numerical results in Fig. 6: 1) with fixed η, it is clear that the value of PEE limits data rate which especially exhibits a performance floor at high SINR regime; 2) with fixed $\Delta\phi$, we also find that if more power is allocated

to cellular user in this system, i.e. η is larger, the system will have a better immunity against PEE induced interference.

V. Case II: Bidirectional D2D Spectrum Sharing and Performance Results

In Case II, only one DU, say D_1, correctly decodes the data packets from BS. Thus, D_1 relays the cellular data and D_2 only transmits its own data. The symbols are thus precoded and given by

$$x_{B,II}^{(n)} = \Re\{s_B^{(n)}\}e^{-\angle h_C} \tag{66}$$

$$x_{\alpha,II}^{(n)} = \begin{cases} \frac{1}{\sqrt{2}}\left(\Re\{s_B^{(n-1)}\} - j\Re\{s_\alpha^{(n)}\}\right)e^{-\angle h_C\alpha}, & \alpha = 1, \\ -j\frac{1}{\sqrt{2}}\Re\{s_\alpha^{(n)}\}e^{-\angle h_C\alpha}, & \alpha = 2, \end{cases}$$
$$= \frac{1}{\sqrt{2}}\left((2-\alpha)\,\Re\{s_B^{(n-1)}\} - j\Re\{s_\alpha^{(n)}\}\right)e^{-\angle h_C\alpha}, \tag{67}$$

where $\alpha = \mathrm{mod}\ (n, 2)$.

Denoting signals received by CU and D_β ($\beta = 3-\alpha$) as $y_C^{(n)}$ and $y_\beta^{(n)}$, we have

$$y_{C,II}^{(n)} = h_C\sqrt{P_B}x_{B,II}^{(n)} + h_{C\alpha}\sqrt{P_D}x_{\alpha,II}^{(n)} + N_C^{(n)}$$
$$= \frac{1}{\sqrt{2}}\left(r_{1,C,II}^{(n)} - jr_{2,C,II}^{(n)}\right), \tag{68}$$

$$y_{\beta,II}^{(n)} = h_{B\beta}\sqrt{P_B}x_{B,II}^{(n)} + h_D\sqrt{P_D}x_{\alpha,II}^{(n)} + N_\beta^{(n)},$$
$$= \frac{1}{\sqrt{2}}\left(r_{1,\beta,II}^{(n)} - jr_{2,\beta,II}^{(n)}\right) + N_\beta^{(n)}, \tag{69}$$

where $r_{1,C,II}^{(n)}$ and $r_{2,C,II}^{(n)}$ are real values given by

$$r_{1,C,II}^{(n)} = |h_C|\sqrt{2P_B}\Re\{s_B^{(n)}\} + (2-\alpha)|h_{C\alpha}|\sqrt{P_D}\Re\{s_B^{(n-1)}\} + \sqrt{2}\Re\{N_C^{(n)}\}, \tag{70}$$

$$r_{2,C,II}^{(n)} = |h_{C\alpha}|\sqrt{P_D}\Re\{s_\alpha^{(n)}\} - \sqrt{2}\Im\{N_C^{(n)}\}, \tag{71}$$

and $r_{1,\beta,II}^{(n)}$ and $r_{2,\beta,II}^{(n)}$ are complex values given by

$$r_{1,\beta,II}^{(n)} = \widetilde{h}_{B\beta}\sqrt{2P_B}\Re\{s_B^{(n)}\} + (2-\alpha)\widetilde{h}_D\sqrt{P_D}\Re\{s_B^{(n-1)}\}, \tag{72}$$

$$r_{2,\beta,II}^{(n)} = \widetilde{h}_D\sqrt{P_D}\Re\{s_\alpha^{(n)}\}. \tag{73}$$

A. Protocol

- Time slot 1: the BS broadcasts its precoded data $x_{B,II}^{(1)} = f_1(s_B^{(1)})$ to the DUs and C_2.
- Time slot 2: the BS transmits precoded signal $x_{B,II}^{(2)} = f_2(s_B^{(2)})$ as (66); D_1 applies the precoding in (67) and transmits the composite signal $x_{1,II}^{(2)} = g(s_B^{(1)}, s_1^{(2)})$; C_2 detects $s_B^{(2)}$ via Theorem 1 and space-time processing (Section V-B); D_2 detects $s_1^{(2)}$ via Theorem 1 and SIC (Section V-C).
- Time slot 3: the BS transmits precoded signal $x_{B,II}^{(3)} = f_2(s_B^{(3)})$ as (66); D_2 applies the precoding in (67) and transmits the composite signal $x_2^{(3)} = g_2(0, s_2^{(3)})$; C_2 detects $s_B^{(3)}$ via Theorem 1 and space-time processing in Section V-B; D_1 detects $s_B^{(3)}$ and $s_2^{(3)}$ via Theorem 1 and SIC technique (Section V-C).
- The progress of time slot 2 and time slot 3 repeats alternatively until time slot L.
- Time slot $L+1$: D_α applies the precoding in (5) and transmits the signal $x_\alpha^{(L+1)} = g(s_B^{(L)}, s_\alpha^{(L+1)})$.

By exploiting the special signal space structure (Theorem 1), both DUs and CUs can decode the cellular and D2D data separately (D_2 separates the cellular data contained in the signal from D_1).

B. Space-Time Processing at CU

Using Rule-1 of Theorem 1, $r_{1,C,II}^{(n)}$ and $r_{2,C,II}^{(n)}$ in (68) can be separated using (1). To decode cellular data from $r_{1,C,II}^{(n)}$, we rewrite all the $r_{1,C,II}^{(n)}$ in $L+1$ time slots as

$$\boldsymbol{r}_{1,C,II} = \mathbf{H}_{II}\boldsymbol{s}_B + \boldsymbol{N}_C, \tag{74}$$

where $\mathbf{H}_{II}$ can be derived from $\mathbf{H}$ in (15) by applying $C_2 = 0$.

$$\mathbf{H}_{II} = \begin{bmatrix} C_B & 0 & \cdots & 0 & 0 \\ C_1 & C_B & \ddots & 0 & 0 \\ 0 & 0 & \ddots & 0 & 0 \\ \vdots & \vdots & \ddots & \vdots & \vdots \\ 0 & 0 & \cdots & C_1 & C_B \\ 0 & 0 & \cdots & 0 & 0 \end{bmatrix}. \tag{75}$$

After replacing $\mathbf{H}$ by $\mathbf{H}_{II}$, the results for forward decoding in (16) or Babai estimator [39] can be applied in this Case. Then the final data detection can be derived from (18) after replacing $\mathbf{H}$ by $\mathbf{H}_{II}$.

C. Decoding at CU and the Feasible Region for D2D Power Scale Coefficient

Using Rule-2 of Theorem 1, $r_{1,\beta,II}$ and $r_{2,\beta,II}$ in (69) can be separated using complex field network coding. For example, it is easy to decode $s_\alpha^{(n)}$ from (73).

When $\alpha = 2$, $r_{1,\beta,II}^{(n)} = \widetilde{h}_{B\beta}\sqrt{2P_B}\Re\{s_B^{(n)}\}$. Thus, decoding $s_B^{(n)}$ from $r_{1,\beta,II}^{(n)}$ is simple.

When $\alpha = 1$, $r_{1,\beta,II}^{(n)}$ equals $r_{1,\beta}^{(n)}$ in (12). Thus, decoding $s_B^{(n)}$ from (72) is the same as the method in Section III-C. Considering this SIC method, the feasible region for D2D power scale coefficient η equals that derived in Section III-D.

D. Performance Results

1) Diversity-Multiplexing Tradeoff Analysis for CU: Conditioned D_1 correctly decoding the message, Case II mimics a multiple access MIMO channel (75). To characterize the achievable DMT, similar to [36] we consider an $(m+1)\times m$ MIMO channel matrix $\mathbf{H}_m$ in the same form as (75). Furthermore, let $\mathbf{M}_{m+1} = \mathbf{I}_{m+1} + \frac{1}{2}\Sigma_S\Sigma_n^{-1}$, where $\sum_S$ and $\sum_n$ denote the covariance matrices of observed signal and noise components at the receiver, respectively. We assume that each source message s_B^n is chosen from a Gaussian random codebook of codeword length l.

As shown in Appendix III, the upper bound on the ML conditional pair-wise error probability can be calculated by

$$P_{PE|v_C,v_{C1}} \le \det\left(\mathbf{I}_{m+1} + \frac{1}{2}\Sigma_S\Sigma_n^{-1}\right)^{-l}$$
$$= \left(1 + \frac{P_Bh_C^4}{4\sigma^4} + \frac{P_Bh_C^2}{\sigma^2} + \frac{P_Dh_{C1}^2}{4\sigma^2}\right)^{-\frac{m}{2}l}$$
$$\doteq \mathrm{SINR}^{-\frac{m}{2}l(\max\{2(1-v_C),1-v_{C1}\})^+}, \tag{76}$$

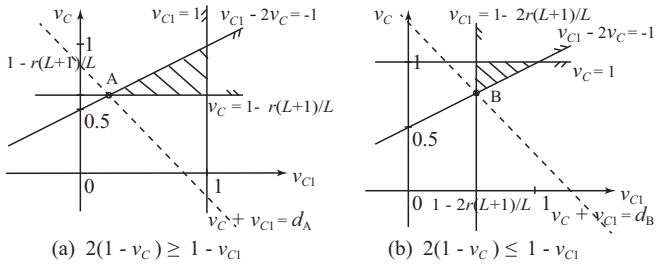

Fig. 7. Linear programming (LP) for calculating $d_o(r)$. For each case, the dashed line denotes the final translation location for the objective function. Both the optimal solutions (A and B) for two cases both $\left(1-2\frac{L+1}{L}r, 1-\frac{L+1}{L}r\right)$. Thus, $d_{\rm A}=d_{\rm B}=1-2\frac{L+1}{L}r+1-\frac{L+1}{L}r=2-3\frac{L+1}{L}r$ is the optimum of LP.

where $\doteq$ denotes asymptotic equality in the high SNR regime, and $\dot{\leq}$, $\dot{\geq}$ are similarly defined.

We assume each s_B^n is transmitted with data rate R bit per channel use (BPCU). Since it takes $L+1$ time slots to transmit L symbols, the average transmission rate is $\overline{R}=\frac{L}{L+1}$. On assuming that average transmission rate changes as $\overline{R}=r\log_2(\text{SINR})$ with respect to SINR, then we get $R=\frac{L+1}{L}r\log_2(\text{SINR})$. Therefore, we have a total of $\text{SINR}^{\frac{L+1}{L}rml}$ codewords. Thus, the error probability can be bounded by

$$P_{E|v_{C0},v_{C1}}\dot{\leq}\text{SINR}^{-l\left(\frac{m}{2}(\max\{2(1-v_C),1-v_{C1}\})^+-\frac{L+1}{L}rm\right)}. \quad (77)$$

Next, we identify the outage events that dominate the error probability, i.e.,

$$P_E\dot{\leq}P_O. \quad (78)$$

Please see Appendix IV for details, and this set is given by

$$O^+=\{(v_C,v_{C1})\in\mathbb{R}^{2+}\Big|\big(\max\{2(1-v_C),(1-v_{C1})\}\big)^+\leq\frac{2(L+1)}{L}r\Big\}. \quad (79)$$

Now using (79), (111) and linear programming (see Fig. 7), $d_o(r)$ can be calculated as

$$d_o(r)=2\left(1-\frac{3}{2}\frac{L+1}{L}r\right)^+, \quad (80)$$

Remark 6. *The closed-form expression of the achievable DMT (80) indicates that the proposed D2D aided two-hop cellular transmission achieves a multiplexing gain of $\frac{2}{3}\frac{L}{L+1}$, which converges to $\frac{2}{3}$ as $L\to\infty$. The single relay aided cellular transmission achieves a full diversity of two. As shown in Fig. 8, although there is a gap between the DMT performance and 2×1 MISO upper bound, the diversity is improved, compared with cellular direct transmission and half-duplex DF relaying. Although the maximum multiplexing gain $\frac{2}{3}$ is inferior to direct transmission and Case I, it is superior to that of half-duplex DF relaying.*

2) SEP and Throughput with HCFNC for DU: Comparing (69) with (9), we find that the difference uniquely exists between $r_{2,\beta}^{(n)}$ and $r_{2,\beta,II}^{(n)}$. Thus, we can adopt the SEP and throughput from the results of Case I.

Eq. (69) can be rewritten as

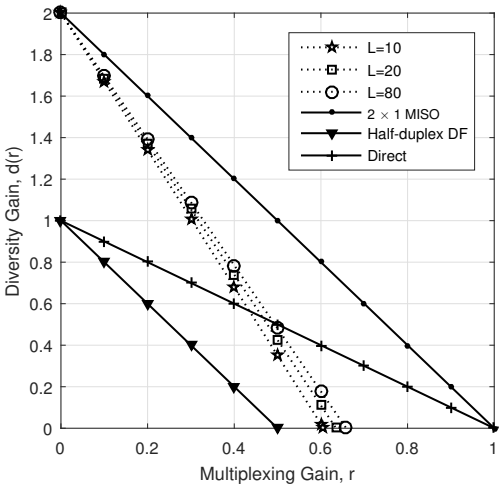

Fig. 8. DMT performance for CU in Case II. The DMT curves for our proposed scheme are shown in dot lines.

$$y_{\beta,II}^{(n)}=X_{II}^{(n)}+N_\beta^{(n)}, \quad (81)$$

where $X_{II}^{(n)}=\frac{1}{\sqrt{2}}\left(u_{1,II}^{(n)}-ju_{2,II}^{(n)}\right)$, $X_{II}^{(n)}\in A_{X,II}$, $u_{1,II}^{(n)}=\widetilde{h}_{B\beta}\sqrt{2P_B}\Re\{s_B^{(n)}\}+(2-\alpha)\widetilde{h}_D\sqrt{P_D}\Re\{s_B^{(n-1)}\}$, $u_{2,II}^{(n)}=\widetilde{h}_D\sqrt{P_D}\Re\{s_\alpha^{(n)}\}$. Assuming $X_a^{(n,II)}$ and $X_b^{(n,II)}$ are two realizations for $X^{(n)}$, and $\boldsymbol{u}_{a,II}^{(n)}$ and $\boldsymbol{u}_{b,II}^{(n)}$ are two realizations for $\boldsymbol{u}_{II}^{(n)}=[u_{1,II}^{(n)},u_{2,II}^{(n)}]^{\rm T}$, the SEP of $X_{II}^{(n)}$ is given by

$$P_{e,II}^{(n)}\leq\frac{1}{2N_n}\sum_{k=1}^{2}k\sum_{a=1}^{N_{n,II}}\left(\sum_{\|\boldsymbol{u}_{a,II}^{(n)}-\boldsymbol{u}_{b,II}^{(n)}\|_0=k}^{N_{n,II}}Q\left(\frac{d_{ab}^{X_{II}^{(n)}}}{2\sqrt{\sigma^2}}\right)\right), \quad (82)$$

where $N_{n,II}=|A_{X,II}|$ and $d_{ab}^{X_{II}^{(n)}}$ denotes the Euclidean distance between $X_{a,II}^{(n)}$ and $X_{b,II}^{(n)}$ in the constellation of $X_{II}^{(n)}$.

Define the throughput $T^{(n)}$ of the D2D link as the average number of successfully transmitted symbols in one time slot. The average throughput of the D2D link over $L+1$ time slots can then be given by

$$T_{D,II}\geq\frac{1}{L+1}\times\sum_{n=2}^{L+1}\left(1-\frac{1}{2N_{n,II}}\sum_{k=1}^{2}k\sum_{a=1}^{N_{n,II}}\left(\sum_{\|\boldsymbol{u}_{a,II}^{(n)}-\boldsymbol{u}_{b,II}^{(n)}\|_0=k}^{N_{n,II}}Q\left(\frac{d_{ab}^{X_{II}^{(n)}}}{2\sqrt{\sigma^2}}\right)\right)\right). \quad (83)$$

Remark 7. *Similar with Remark 3, the lower bound for DU throughput (43), approximated as $\frac{L}{L+1}$ in high SINR regime, approaches 1 sym/TS. Then, DU can access cellular spectrum in each time slot to exchange its data for local services, which infers that D2D system gains full spectrum access opportunity. The numerical results in Fig. 9 verify the analysis, and show that the performance of Case II is inferior to Case I. This can be explained by the difference between $r_{2,\beta}^{(n)}$ and $r_{2,\beta,II}^{(n)}$, which differs the variances of $d_{ab}^{X^{(n)}}$ and $d_{ab}^{X_{II}^{(n)}}$. In BPSK comparison, both of our schemes can achieve higher D2D spectrum access*

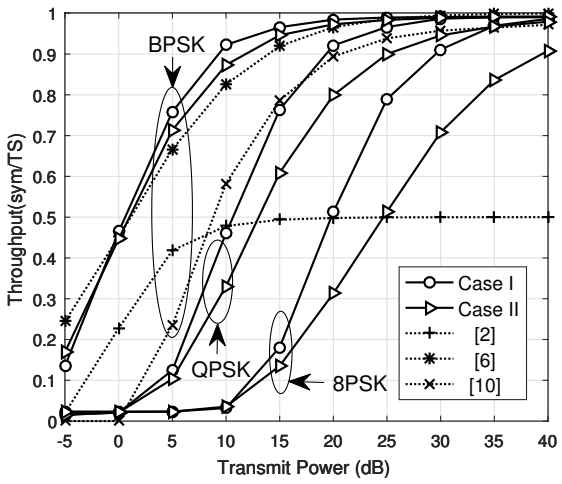

Fig. 9. The average throughput for DU in Case II compared with Case I. Simulation parameters are set the same with Fig. 3.

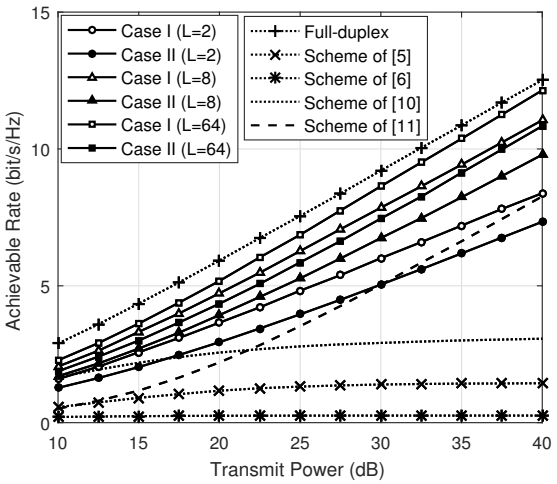

Fig. 10. Achievable rate for CU in Case II compared with Case I. Simulation parameters are set the same with Fig. 4.

opportunity than three previous works.

3) Achievable Rate for CU Channel: the achievable rate for the broadcast phase can be calculated as

$$R_{C,II} = \frac{1}{L+1}\log_2\left(\det\left(\boldsymbol{I}_{L+1} + \frac{1}{\sigma^2}\mathbf{H}_{II}\mathbf{H}_{II}^{\mathrm{H}}\right)\right) = \frac{1}{L+1}\log_2|\mathbf{M}_{II}| \quad \text{(bit/s/Hz)}, \tag{84}$$

where $\mathbf{M}_{II}$ is given by

$$\mathbf{M}_{II} = \begin{bmatrix} \mathbf{B}_4 & \mathbf{0}_4 & \cdots & \mathbf{0}_4 & \boldsymbol{0}_2 \\ \mathbf{0}_4 & \mathbf{B}_4 & \cdots & \mathbf{0}_4 & \boldsymbol{0}_2 \\ \vdots & \vdots & \ddots & \vdots & \vdots \\ \mathbf{0}_4 & \mathbf{0}_4 & \cdots & \mathbf{B}_4 & \boldsymbol{0}_2 \\ \boldsymbol{0}_2^T & \boldsymbol{0}_2^T & \cdots & \boldsymbol{0}_2^T & 1 \end{bmatrix}, \tag{85}$$

with $\mathbf{B}_4 = \begin{bmatrix} 1+\frac{C_B^2}{\sigma^2} & \frac{C_1C_B}{\sigma^2} \\ \frac{C_1C_B}{\sigma^2} & 1+\frac{C_1^2+C_B^2}{\sigma^2} \end{bmatrix}$, $\mathbf{0}_4 = \begin{bmatrix} 0 & 0 \\ 0 & 0 \end{bmatrix}$, and $\boldsymbol{0}_2 = [0,0]^T$. Then, R_C can be calculated by

$$R_{C,II} = \frac{1}{L+1}\log_2|\mathbf{B}_4|^{\frac{L}{2}} = \frac{L}{2(L+1)}\log_2|\mathbf{B}_4|, \tag{86}$$

where $|\mathbf{B}_4| = \left(1+\frac{C_B^2}{\sigma^2}\right)^2 + \frac{C_1^2}{\sigma^2} = \left(1+\frac{P_B g_c}{\sigma^2}\right)^2 + \frac{P_D g_{C1}}{\sigma^2}$. As $L \in (2,\infty)$, the bounds for $R_{C,II}$ exist:

$$\frac{1}{3}\log_2|\mathbf{B}_4| < R_{C,II} < \frac{1}{2}\log_2|\mathbf{B}_4|. \tag{87}$$

Remark 8. *The numerical results in Fig. 10 show that the CU achievable rate in Case II is rather inferior to that of Case I. This is because only one DU in Case II is utilized to relay CU message. Consider that CU in Case II broadcasts its data in each time slot. On one hand, multiplexing gain is higher than $\frac{1}{2}$ and thus the data rate is higher than half-duplex relaying system, if the channel condition of direct-path is good enough. On the other hand, half of the data broadcast by DU is not protected by the diversity, because half of these data are only forwarded by cellular direct-path. From the comparison with previous schemes, it is easy to find that choosing larger frame length L can help Case II to outperform other schemes.*

VI. Conclusion

We have proposed a successive spectrum sharing scheme that allows a pair of DUs to fully access cellular spectrum while enhancing the CU capacity. Based on two-path successive relaying, the two DUs forms a 'virtual full-duplex relay' to not only gain their own transmission opportunity via the inter-relay interference channel, but also to support the full-duplex CU transmissions with full diversity. To avoid the intra-cell interference between cellular and D2D links, we proposed a hybrid complex network coding technique which ensures that the CUs have first priority and avoid DU interference. We considered two primary cases depending on whether both DUs are decoding or not, and derived the DMT for cellular link, symbol error probability for HCFNC strategy, and the throughput of the D2D link. Our performance analysis and numerical results show that in Case I: 1) the cellular link achieves the 3×1 MISO DMT with full diversity; 2) the cellular link achieves full-duplex mode even though all DUs are half-duplex; 3) cellular link is interference-free from DU access due to HCFNC; and 4) the cellular priority is guaranteed and cellular users are incentivized for spectrum sharing; 5) DUs gain full spectrum access opportunity. For all these reasons, Case I has the most potential realizability in practice. The performance of Case II depends much on the cellular direct-path, and thus it can be adopted appropriately when D2D access is urgent and the cellular channel is not subject to deep fading. While Case II is a necessary complement to Case I, but if two suitable DUs exist, Case I is a win-win strategy.

Appendix I: Proof of Lemma 1

Eq. (21) can be rewritten as

$$\frac{g_{\max}}{g_{\min}} \geq 2^{R_D^{tar}} - 1. \tag{88}$$

A. $2P_B|h_{B\beta}|^2 \geq P_D|h_D|^2$ *(case-i)*

In this case, we have $g_{\max} = 2P_B|h_{B\beta}|^2$, $g_{\min} = P_D|h_D|^2$ and

$$\eta = \frac{P_D}{P_B} \leq \frac{2|h_{S\beta}|^2}{|h_D|^2}. \tag{89}$$

Considering $g_{\max}$ and $g_{\min}$, the inequality for η can be derived from (88) as

$$\eta \leq \frac{1}{2^{R_D^{tar}}-1}\frac{2|h_{S\beta}|^2}{|h_D|^2}. \tag{90}$$

Thus, we have the following feasible region

$$0<\eta\leq\begin{cases}\frac{2|h_{S\beta}|^2}{|h_D|^2}, & 0<R_D^{tar}\leq 1,\\ \frac{1}{2^{R_D^{tar}}-1}\frac{2|h_{S\beta}|^2}{|h_D|^2}, & R_D^{tar}>1.\end{cases} \tag{91}$$

B. $2P_B|h_{B\beta}|^2 \leq P_D|h_D|^2$ *(case-ii)*

In this case, we have $g_{\max} = P_D|h_D|^2$, $g_{\min} = 2P_B|h_{B\beta}|^2$ and

$$\eta = \frac{P_D}{P_B} \geq \frac{2|h_{S\beta}|^2}{|h_D|^2}. \tag{92}$$

Considering $g_{\max}$ and $g_{\min}$, the inequality for η can be derived from (88) as

$$\eta \geq \left(2^{R_D^{tar}}-1\right)\frac{2|h_{S\beta}|^2}{|h_D|^2}. \tag{93}$$

Then, we have the following feasible region

$$\eta\geq\begin{cases}\frac{2|h_{S\beta}|^2}{|h_D|^2}, & 0<R_D^{tar}\leq 1,\\ \left(2^{R_D^{tar}}-1\right)\frac{2|h_{S\beta}|^2}{|h_D|^2}, & R_D^{tar}>1.\end{cases} \tag{94}$$

Based on the results of *case-i* and *case-ii*, the feasible region for η is given by

$$\eta\in\begin{cases}\mathbb{R}^+, & 0<R_D^{tar}\leq 1,\\ (0,\frac{G}{2^{R_D^{tar}}-1}]\bigcup[(2^{R_D^{tar}}-1)G,\infty), & R_D^{tar}>1,\end{cases} \tag{95}$$

where $G = \frac{2|h_{S\beta}|^2}{|h_D|^2}$.

Appendix II: Derivation of (59)

The normalized equivalent MIMO channel (58) is approximated by

$$\widetilde{\mathbf{H}}_c \approx \begin{bmatrix}\widetilde{\mathbf{H}}_0 & & & \\ & \widetilde{\mathbf{H}}_1 & & \\ & & \ddots & \\ & & & \widetilde{\mathbf{H}}_1\end{bmatrix}, \tag{96}$$

where

$$\widetilde{\mathbf{H}}_0 = \begin{bmatrix}\frac{\widetilde{C}_B}{\sigma} & 0\\ \frac{\widetilde{C}_1}{\sqrt{\lambda_1}} & \frac{\widetilde{C}_B}{\sqrt{\lambda_1}}\\ 0 & \frac{\widetilde{C}_2}{\sqrt{\lambda_2}}\end{bmatrix},\ \widetilde{\mathbf{H}}_1 = \begin{bmatrix}\frac{\widetilde{C}_B}{\sqrt{\lambda_2}} & 0\\ \frac{\widetilde{C}_1}{\sqrt{\lambda_1}} & \frac{\widetilde{C}_B}{\sqrt{\lambda_1}}\\ 0 & \frac{\widetilde{C}_2}{\sqrt{\lambda_2}}\end{bmatrix}. \tag{97}$$

We evaluate the determinant of the tridiagonal martix as [12]

$$\det\left(\boldsymbol{I}_{L+1}+\widetilde{\mathbf{H}}_c\widetilde{\mathbf{H}}_c^{\mathrm{H}}\right)\approx|B_1|\cdot|B_2|^{\frac{L-2}{2}}, \tag{98}$$

where $|B_1| = \det\left(I_3+\widetilde{\mathbf{H}}_0\widetilde{\mathbf{H}}_0^{\mathrm{H}}\right) = 1+\frac{\widetilde{C}_1^2}{\lambda_1}+\frac{\widetilde{C}_B^2}{\lambda_1}+\frac{\widetilde{C}_2^2}{\lambda_2}+\frac{\widetilde{C}_1^2\widetilde{C}_2^2}{\lambda_1\lambda_2}+\frac{\widetilde{C}_B^2}{\sigma^2}+\frac{\widetilde{C}_B^4}{\lambda_1\sigma^2}+\frac{\widetilde{C}_2^2\widetilde{C}_B^2}{\lambda_2\sigma^2}$ and $|B_2| = \det\left(I_3+\widetilde{\mathbf{H}}_1\widetilde{\mathbf{H}}_1^{\mathrm{H}}\right) = 1+\frac{\widetilde{C}_1^2}{\lambda_1}+\frac{\widetilde{C}_B^2}{\lambda_1}+\frac{\widetilde{C}_2^2}{\lambda_2}+\frac{\widetilde{C}_1^2\widetilde{C}_2^2}{\lambda_1\lambda_2}+\frac{\widetilde{C}_B^2}{\lambda_2}+\frac{\widetilde{C}_B^4}{\lambda_1\lambda_2}+\frac{\widetilde{C}_2^2\widetilde{C}_B^2}{\lambda_2^2}$. Then, the achievable rate can be approximated by

$$\begin{aligned}\widetilde{R}_C' &= \frac{1}{L+1}\log_2\left\{|B_1|\cdot|B_2|^{\frac{L-2}{2}}\right\}\\ &= \frac{1}{2}\log_2|B_2|+\frac{1}{L+1}\Delta\widetilde{R},\end{aligned} \tag{99}$$

where $\Delta\widetilde{R} = \log_2\left(|B_1||B_2|^{-\frac{3}{2}}\right)$.

Appendix III: Derivation of (76)

$$\Sigma_n^{-1} = \frac{1}{\sigma^2}\mathbf{I}_{m+1}, \tag{100}$$

$$\Sigma_{S|C_B,C_1}=\begin{bmatrix}C_B^2 & 0 & 0 & \cdots & 0 & 0 & 0\\ C_1C_B & C_B^2 & 0 & \cdots & 0 & 0 & 0\\ 0 & 0 & C_B^2 & \cdots & 0 & 0 & 0\\ \vdots & \vdots & \vdots & \ddots & \vdots & \vdots & \vdots\\ 0 & 0 & 0 & \cdots & C_B^2 & 0 & 0\\ 0 & 0 & 0 & \cdots & 0 & C_B^2 & 0\\ 0 & 0 & 0 & \cdots & 0 & C_1C_B & C_B^2\\ 0 & 0 & 0 & \cdots & 0 & 0 & 0\end{bmatrix}, \tag{101}$$

$$\mathbf{M}_{m+1|C_B,C_1} = \begin{bmatrix}\mathbf{H}_4 & \mathbf{0}_4 & \cdots & \mathbf{0}_4 & \boldsymbol{0}_2\\ \mathbf{0}_4 & \mathbf{H}_4 & \cdots & \mathbf{0}_4 & \boldsymbol{0}_2\\ \vdots & \vdots & \ddots & \vdots & \vdots\\ \mathbf{0}_4 & \mathbf{0}_4 & \cdots & \mathbf{H}_4 & \boldsymbol{0}_2\\ \boldsymbol{0}_2^T & \boldsymbol{0}_2^T & \cdots & \boldsymbol{0}_2^T & 1\end{bmatrix}, \tag{102}$$

where $\mathbf{H}_4 = \begin{bmatrix}1+\frac{C_B^2}{4\sigma^2} & \frac{C_1C_B}{4\sigma^2}\\ \frac{C_1C_B}{4\sigma^2} & 1+\frac{C_1^2+C_B^2}{4\sigma^2}\end{bmatrix}$, $\mathbf{0}_4 = \begin{bmatrix}0 & 0\\ 0 & 0\end{bmatrix}$, and $\boldsymbol{0}_2 = [0,0]^T$. Thus, considering $C_B = \sqrt{2P_B}|h_C|$ and $C_1 = \sqrt{P_D}|h_{C1}|$, (76) can be rewritten as

$$\begin{aligned}P_{PE|C_B,C_1} &\leq \left|\left(\mathbf{M}_{m+1|C_B,C_1}\right)\right|^l = \left(1\cdot|\mathbf{H}_4|^{\frac{m}{2}}\right)^{-l}\\ &= \left(1+\frac{P_Bh_C^4}{4\sigma^4}+\frac{P_Bh_C^2}{\sigma^2}+\frac{P_Dh_{C1}^2}{4\sigma^2}\right)^{-\frac{m}{2}l}.\end{aligned} \tag{103}$$

Based on $h_C^2 \doteq \mathrm{SINR}^{-v_C}$, $h_{C1}^2 \doteq \mathrm{SINR}^{-v_{C1}}$ and $P_D = \eta P_B$, we can further derive

$$\begin{aligned}P_{PE|v_C,v_{C1}} &\leq \left(1+\frac{P_Bh_C^4}{4\sigma^4}+\frac{P_Bh_C^2}{\sigma^2}+\frac{P_Dh_{C1}^2}{4\sigma^2}\right)^{-\frac{m}{2}l}\\ &\doteq \left(\frac{\mathrm{SINR}^{2(1-v_C)}}{4}+\frac{\eta\mathrm{SINR}^{1-v_{C1}}}{4}\right)^{-\frac{m}{2}l}\\ &\doteq \mathrm{SINR}^{-\frac{ml}{2}(\max\{2(1-v_C),1-v_{C1}\})^+}.\end{aligned} \tag{104}$$

Appendix IV: Analysis regarding (78) and (79)

The event corresponding to $P_{E|v_C,v_{C1}}$ contains O and O^c, where O denotes the outage event, and O^c denotes the non-outage event. Using Bayes' rule, P_E can be upper-bounded as

$$P_E = P_OP_{E|O}+P_{E,O^c} \leq P_O+P_{E,O^c}. \tag{105}$$

Thus, (78) can be guaranteed, if the outage event O is chosen such that P_O dominates P_{E,O^c}, i.e.,

$$P_{E,O^c} \dot{\leq} P_O. \tag{106}$$

In order to characterize O ensuring (106), we should examine the probability $P_{E|O^c}$

$$P_{E,O^c} = \int_{o^{c+}} P_{E,O|v_C,v_{C1}} f_{v_C} f_{v_{C1}} dv_C dv_{C1}, \quad (107)$$

where $f_{v_C} \doteq \text{SINR}^{-v_C}$ and $f_{v_{C1}} \doteq \text{SINR}^{-v_{C1}}$ [45] are the probability density function (pdf) of v_C and v_{C1} respectively. Using (77), (107) can be rewritten as

$$\begin{aligned} P_{E,O^c} &\doteq \int_{o^{c+}} P_{E,O|v_C,v_{C1}} \text{SINR}^{-(v_C+v_{C1})} dv_C dv_{C1}, \\ &\dot{\leq} \int_{o^{c+}} \text{SINR}^{-d_e(r,v_C,v_{C1})} dv_C dv_{C1}, \end{aligned} \quad (108)$$

for

$$\begin{aligned} d_e(r, v_C, v_{C1}) &= (v_C + v_{C1}) + ml \times \\ &\left(\frac{1}{2} \left(\max\{2(1-v_C), 1-v_{C1}\} \right)^+ - \frac{L+1}{L} r \right). \end{aligned} \quad (109)$$

Now P_{E,O^c} is dominated by the term corresponding to the minimum value of $d_e(r, v_C, v_{C1})$ over O^{c+}:

$$P_{E,O^c} \dot{\leq} \text{SINR}^{-d_e(r)} \text{ for } d_e(r) = \inf_{v_C, v_{C1} \in O^{c+}} d_e(r, v_C, v_{C1}). \quad (110)$$

The outage probability P_O can be expressed as [45]

$$P_O \doteq \text{SINR}^{d_o(r)} \text{ for } d_o(r) = \inf_{(v_C, v_{C1}) \in O^+} (v_C + v_{C1}). \quad (111)$$

Comparing (110) and (111), we note that for (106) to be satisfied, O^+ should be chosen as

$$\begin{aligned} O^+ = \{(v_C, v_{C1}) \in \mathbb{R}^{2+} \Big| \big(&\max\{2(1-v_C), \\ &(1-v_{C1})\}\big)^+ \leq \frac{2(L+1)}{L} r \Big\}. \end{aligned}$$

For $\forall (v_C, v_{C1}) \in O^{c+}$, it is possible to choose m or l to make $d_e(r, v_C, v_{C1})$ arbitrarily large, satisfying (106). Thus, (78) can be guaranteed by choosing $(v_C, v_{C1}) \in O^{c+}$, which means the error performance is dominated by the outage probability.

REFERENCES

[1] K. Doppler, M. Rinne, C. Wijting, C. Ribeiro, and K. Hugl, "Device-to-device communication as an underlay to LTE-advanced networks," *IEEE Commun. Mag.*, vol. 47, no. 12, pp. 42–49, Dec. 2009.

[2] C. Ma, G. Sun, X. Tian, K. Ying, Y. Hui, and X. Wang, "Cooperative relaying schemes for device-to-device communication underlaying cellular networks," in *Proc. IEEE GLOBECOM*, 2013, pp. 3890–3895.

[3] X. Lin, R. Ratasuk, and A. Ghosh, "Network-assisted device-to-device scheduling in LTE," in *Proc. IEEE Veh. Technol. Conf.*, 2015, pp. 1–5.

[4] G. Fodor, E. Dahlman, G. Mildh, S. Parkvall, N. Reider, G. Miklos, and Z. Turanyi, "Design aspects of network assisted device-to-device communications," *IEEE Commun. Mag.*, vol. 50, no. 3, pp. 170–177, Mar. 2012.

[5] D. T. Ngo, C. Tellambura, and H. H. Nguyen, "Efficient resource allocation for ofdma multicast systems with spectrum-sharing control," *IEEE Trans. on Vehi. Tech.*, vol. 58, no. 9, pp. 4878–4889, 2009.

[6] X. Gong, S. A. Vorobyov, and C. Tellambura, "Joint bandwidth and power allocation with admission control in wireless multi-user networks with and without relaying," *IEEE Trans. Signal Proc.*, vol. 59, no. 4, pp. 1801–1813, 2011.

[7] G. Zhang, K. Yang, P. Liu, and J. Wei, "Power allocation for full-duplex relaying-based D2D communication underlaying cellular networks," *IEEE Trans. Veh. Technol.*, vol. 64, no. 10, pp. 4911–4916, Oct. 2015.

[8] Y. Pei and Y. chang Liang, "Resource allocation for device-to-device communications overlaying two-way cellular networks," *IEEE Trans. Wireless Commun.*, vol. 12, no. 7, pp. 3611–3621, Jul. 2013.

[9] ——, "Cooperative spectrum sharing with bidirectional secondary transmissions," *IEEE Trans. Veh. Technol.*, vol. 64, no. 1, pp. 108–117, Jan. 2015.

[10] M. Song, C. Xin, Y. Zhao, and X. Cheng, "Dynamic spectrum access: From cognitive radio to network radio," *IEEE Wireless Commun. Mag.*, vol. 19, no. 1, pp. 23–29, Feb. 2012.

[11] P. Li and S. Guo, "Incentive mechanisms for device-to-device communications," *IEEE Netw.*, vol. 29, no. 4, pp. 75–79, Jul. 2015.

[12] C. Zhai, W. Zhang, and P. Ching, "Cooperative spectrum sharing based on two-path successive relaying," *IEEE Trans. Commun.*, vol. 61, no. 6, pp. 2260–2270, Jun. 2013.

[13] L. Sun, Q. Du, P. Ren, and Y. Wang, "Two birds with one stone: Towards secure and interference-free D2D transmissions via constellation rotation," *IEEE Trans. Veh. Technol.*, vol. 65, no. 10, pp. 8767–8774, Oct. 2016.

[14] G. Amarasuriya, M. Ardakani, and C. Tellambura, "Output-threshold multiple-relay-selection scheme for cooperative wireless networks," *IEEE Trans. Veh. Tech.*, vol. 59, no. 6, pp. 3091–3097, 2010.

[15] G. Amarasuriya, C. Tellambura, and M. Ardakani, "Performance analysis of hop-by-hop beamforming for dual-hop MIMO AF relay networks," *IEEE Trans. Commun.*, vol. 60, no. 7, pp. 1823–1837, Jul. 2012.

[16] S. Atapattu, Y. Jing, H. Jiang, and C. Tellambura, "Relay selection and performance analysis in multiple-user networks," *IEEE J. Sel. Areas Commun.*, vol. 31, no. 8, pp. 1517–1529, Aug. 2013.

[17] F. Zhou, N. C. Beaulieu, Z. Li, J. Si, and P. Qi, "Energy-efficient optimal power allocation for fading cognitive radio channels: Ergodic capacity, outage capacity, and minimum-rate capacity," *IEEE Trans. Wirel. Commun.*, vol. 15, no. 4, pp. 2741–2755, Apr. 2016.

[18] R. Krishnan, A. Graell i Amat, T. Eriksson, and G. Colavolpe, "Constellation optimization in the presence of strong phase noise," *IEEE Trans. Commun.*, vol. 61, no. 12, pp. 5056–5066, Dec. 2013.

[19] N. Devroye, P. Mitran, and V. Tarokh, "Achievable rates in cognitive radio channels," *IEEE Trans. Inf. Theory*, vol. 52, no. 5, pp. 1813–1827, May 2006.

[20] ——, "Limits on communications in a cognitive radio channel," *IEEE Commun. Mag.*, vol. 44, no. 6, pp. 44–49, Jun. 2006.

[21] B. Zhou, H. Hu, S.-Q. Huang, and H.-H. Chen, "Intracluster device-to-device relay algorithm with optimal resource utilization," *IEEE Trans. Veh. Technol.*, vol. 62, no. 5, pp. 2315–2326, Jun. 2013.

[22] J. Li, M. Lei, and F. Gao, "Device-to-device (D2D) communication in MU-MIMO cellular networks," in *Proc. IEEE GLOBECOM*, 2012, pp. 3583–3587.

[23] G. Amarasuriya, C. Tellambura, and M. Ardakani, "Two-way amplify-and-forward multiple-input multiple-output relay networks with antenna selection," *IEEE J. Sel. Areas Commun.*, vol. 30, no. 8, pp. 1513–1529, Sep. 2012.

[24] M. Ju and I.-M. Kim, "Relay selection with ANC and TDBC protocols in bidirectional relay networks," *IEEE Trans. Commun.*, vol. 58, no. 12, pp. 3500–3511, Dec. 2010.

[25] S. Silva, G. Amarasuriya, C. Tellambura, and M. Ardakani, "Relay selection strategies for MIMO two-way relay networks with spatial multiplexing," *IEEE Trans. on Commun.*, vol. 63, no. 12, pp. 4694–4710, Dec. 2015.

[26] S. H. Kim, T. Chaitanya, T. Le-Ngoc, and J. Kim, "Rate maximization based power allocation and relay selection with IRI consideration for two-path AF relaying," *IEEE Trans. Wirel. Commun.*, vol. 14, no. 11, pp. 6012–6027, Nov. 2015.

[27] M. Mohammadi, H. A. Suraweera, Y. Cao, I. Krikidis, and C. Tellambura, "Full-duplex radio for uplink/downlink wireless access with spatially random nodes," *IEEE Trans. Commun.*, vol. 63, no. 12, pp. 5250–5266, Dec. 2015.

[28] C. Ren, J. Chen, Y. Kuo, L. Yang, and L. Lyu, "Three-path successive relaying protocol with blind inter-relay interference cancellation and cooperative non-coherent detection," *Wireless Commun. Mobile Comput.*, vol. 16, no. 17, pp. 2778–2791, Dec. 2016.

[29] C. Ren, J. Chen, Y. Kuo, and L. Yang, "Differential successive relaying scheme for fast and reliable data delivery in vehicular ad hoc networks," *IET Commun.*, vol. 9, no. 8, pp. 1088–1095, May 2015.

[30] L. Sun, T. Zhang, and H. Niu, "Inter-relay interference in two-path digital relaying systems: Detrimental or beneficial?" *IEEE Trans. Wireless Commun.*, vol. 10, no. 8, pp. 2468–2473, Aug. 2011.

[31] C. Zhai, W. Zhang, and P. C. Ching, "Spectrum leasing based on bandwidth efficient relaying in cognitive radio networks," in *Proc. IEEE GLOBECOM*, Dec. 2012, pp. 4927–4932.

[32] C. Zhai and W. Zhang, "Adaptive spectrum leasing with secondary user scheduling in cognitive radio networks," *IEEE Trans. Wirel. Commun.*, vol. 12, no. 7, pp. 3388–3398, Jul. 2013.

[33] C. Luo, Y. Gong, and F. Zheng, "Full interference cancellation for two-path relay cooperative networks," *IEEE Trans. Veh. Technol.*, vol. 60, no. 1, pp. 343–347, Jan. 2011.

[34] *Wireless* LAN *Medium Access Control (*MAC*) and Physical Layer (*PHY*) Specifications: High Speed Physical Layer in the 5* GHz *Band*, IEEE Standard 802.11a, 1999.

[35] *Wireless* LAN *Medium Access Control (*MAC*) and Physical Layer (*PHY*) Specifications: Enhancements for Higher Throughput*, IEEE Standard 802.11nD2.00, 2007.
[36] Y. Fan, C. Wang, J. Thompson, and H. Poor, "Recovering multiplexing loss through successive relaying using repetition coding," *IEEE Trans. Wireless Commun.*, vol. 6, no. 12, pp. 4484–4493, Dec. 2007.
[37] H. Lu, P. Hong, and K. Xue, "High-throughput cooperative communication with interference cancellation for two-path relay in multi-source system," *IEEE Trans. Wireless Commun.*, vol. 12, no. 10, pp. 4840–4851, Oct. 2013.
[38] T. Wang and G. Giannakis, "Complex field network coding for multiuser cooperative communications," *IEEE J. Sel. Areas Commun.*, vol. 26, no. 3, pp. 561–571, Apr. 2008.
[39] J. Wen and X. W. Chang, "Success probability of the Babai estimators for box-constrained integer linear models," *IEEE Trans. Inf. Theory*, vol. 63, no. 1, pp. 631–648, Jan. 2017.
[40] J. Wen, Z. Zhou, J. Wang, X. Tang, and Q. Mo, "A sharp condition for exact support recovery with orthogonal matching pursuit," *IEEE Trans. Signal Process.*, vol. 65, no. 6, pp. 1370–1382, Mar. 2017.
[41] H. Wicaksana, S. Ting, Y. Guan, and X.-G. Xia, "Decode-and-forward two-path half-duplex relaying: Diversity-multiplexing tradeoff analysis," *IEEE Trans. Commun.*, vol. 59, no. 7, pp. 1985–1994, Jul. 2011.
[42] J. Laneman, D. Tse, and G. W. Wornell, "Cooperative diversity in wireless networks: Efficient protocols and outage behavior," *IEEE Trans. Inf. Theory*, vol. 50, no. 12, pp. 3062–3080, Dec. 2004.
[43] R. E. Ziemer and R. L. Peterson, *Introduction to digital communication*. Prentice Hall, 2001.
[44] V. N. Q. Bao, T. Q. Duong, and C. Tellambura, "On the performance of cognitive underlay multihop networks with imperfect channel state information," *IEEE Trans. Commun.*, vol. 61, no. 12, pp. 4864–4873, Dec. 2013.
[45] K. Azarian, H. El Gamal, and P. Schniter, "On the achievable diversity-multiplexing tradeoff in half-duplex cooperative channels," *IEEE Trans. Inf. Theory*, vol. 51, no. 12, pp. 4152–4172, Dec. 2005.

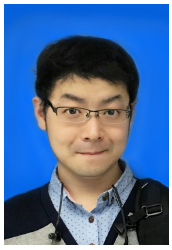

Chao Ren (S'15) received the B.Eng degree in Telecommunications Engineering from Ocean University of China in 2011. He is currently working toward the Ph.D. degree in Telecommunications Engineering at Xidian University. Since September 2016, he has been with the University of Alberta, under the supervision of Prof. Chintha Tellambura, as a joint Ph.D. student sponsored by the China Scholarship Council (CSC). His research interests include cooperative networks, device-to-device communications and full-duplex relaying.

He served as a member of Technical Program Committee (TPC) for 2017 IEEE 86th Vehicular Technology Conference (Fall) on Multiple Antenna Systems and Cooperative Communications.

Jian Chen (M'14) received the B.Eng degree from Xi'an Jiaotong University, China, in 1989, the M.Eng degree from Xi'an Institute of Optics and Precision Mechanics of Chinese Academy of Sciences in 1992, and the Ph.D. degree in Telecommunications Engineering from Xidian University, China, in 2005. He is currently a Full Professor at the School of Telecommunications Engineering, Xidian University. He was a Visiting Scholar with the University of Manchester from 2007 to 2008. His research interests are cognitive radio, physical layer security, wireless sensor networks, compress sensing and signal processing.

Chintha Tellambura (F'11) received the B.Sc. degree (with first-class honor) from the University of Moratuwa, Sri Lanka in 1986, the MSc degree in Electronics from Kings College, University of London, United Kingdom in 1988, and the PhD degree in Electrical Engineering from the University of Victoria, Canada, in 1993.

He was a Postdoctoral Research Fellow with the University of Victoria (1993-1994) and the University of Bradford (1995-1996). He was with Monash University, Australia, from 1997 to 2002. Presently, he is a Professor with the Department of Electrical and Computer Engineering, University of Alberta. His current research interests include the design, modelling and analysis of cognitive radio, heterogeneous cellular networks and 5G wireless networks.

Prof. Tellambura served as an editor for both IEEE Transactions on Communications (1999-2011) and IEEE Transactions on Wireless Communications (2001-2007) and was the Area Editor for Wireless Communications Systems and Theory in the IEEE Transactions on Wireless Communications during 2007-2012. Prof. Tellambura and co-authors received the Communication Theory Symposium best paper award in the 2012 IEEE International Conference on Communications, Ottawa, Canada. He is the winner of the prestigious McCalla Professorship and the Killam Annual Professorship from the University of Alberta. In 2011, he was elected as an IEEE Fellow for his contributions to physical layer wireless communication theory. Prof. Tellambura has authored or coauthored over 500 journal and conference papers with total citations more than 13,000 and an H-index of 59 (Google Scholar).